Protection and Control of
Modern Power Systems

ORIGINAL RESEARCH

Open Access

Novel Lyapunov-based rapid and ripple-free MPPT using a robust model reference adaptive controller for solar PV system

Saibal Manna*, Ashok Kumar Akella and Deepak Kumar Singh

Abstract

The technological, economic, and environmental benefits of photovoltaic (PV) systems have led to their widespread adoption in recent years as a source of electricity generation. However, precisely identifying a PV system's maximum power point (MPP) under normal and shaded weather conditions is crucial to conserving the maximum generated power. One of the biggest concerns with a PV system is the existence of partial shading, which produces multiple peaks in the P–V characteristic curve. In these circumstances, classical maximum power point tracking (MPPT) approaches are prone to getting stuck on local peaks and failing to follow the global maximum power point (GMPP). To overcome such obstacles, a new Lyapunov-based Robust Model Reference Adaptive Controller (LRMRAC) is designed and implemented to reach GMPP rapidly and ripple-free. The proposed controller also achieves MPP accurately under slow, abrupt and rapid changes in radiation, temperature and load profile. Simulation and OPAL-RT real-time simulators in various scenarios are performed to verify the superiority of the proposed approach over the other state-of-the-art methods, i.e., ANFIS, INC, VSPO, and P&O. MPP and GMPP are accomplished in less than 3.8 ms and 10 ms, respectively. Based on the results presented, the LRMRAC controller appears to be a promising technique for MPPT in a PV system.

Keywords Photovoltaic (PV), MPPT, Partial shading, Lyapunov-based robust model reference adaptive control (LRMRAC), Lyapunov stability

1 Introduction

1.1 Aims

The fundamental causes that lead to increase in energy demand worldwide are the improvement in living standards, the considerable development in industry, and substantial population growth. Fossil fuels, e.g., gas, oil, coal etc., will eventually run out [1]. Therefore, it is crucial that the world focuses on discovering new renewable and sustainable sources of energy, with no adverse effects on the environment and guaranteeing a secure future for humanity. The usage of solar photovoltaic (PV) energy has increased dramatically all over the world in recent years. Researchers are currently working to improve PV power output by examining all possible environmental elements that can improve or hamper PV performance [2]. Solar irradiation and temperature have a significant impact on PV energy conversion efficiency. Moreover, harvesting maximum power from a PV system becomes very challenging under partial shading conditions (PSC), which can be caused by anything that reduces or stops the incident radiation from reaching the series modules at the same level [3]. Under uniform weather patterns, there is only one peak in the P–V curve when all the PV modules connected in series get the same amount of solar radiation. However, with PSC, there may be more than one peak at which power is at its highest, and this highest

*Correspondence:
Saibal Manna
mannasaibal1994@gmail.com
Department of Electrical Engineering, National Institute of Technology Jamshedpur, Jharkhand 831014, India

point is the global maximum power point (GMPP), which represents the maximum feasible power harvest from the PV array. High performance can only be achieved if the PV panel's operating point aligns with its MPP. Therefore, it is crucial for a PV system to have MPPT control. Numerous MPPT algorithms, both conventional and soft computing, have been proposed [4, 5].

Much research has been done on incremental conductance (INC) [6] and perturbation and observation (P&O) [7] approaches, which are two of the more common types of traditional MPPT algorithms. The key advantages of these algorithms are their simplicity and low cost, and ability to follow the MPP in uniform weather. However, their main downsides include oscillations generated around the MPP and inefficiency under PSC by restricting to the closest local maximum power point (LMPP). To counter these drawbacks, soft computing MPPT algorithms, such as metaheuristic and artificial intelligence (AI) algorithms, have been presented in the literature. PV performance under PSC is improved using AI methods, i.e., fuzzy logic control (FLC) [8, 9], artificial neural networks (ANN) [10, 11], and metaheuristic MPPT algorithms (e,g., genetic algorithm (GA) [12], particle swarm optimization (PSO) [13]). However, in addition to the complexity of hardware implementation, such artificial intelligence algorithms are expensive, complex, time-consuming to compute, and require prior knowledge to handle. Therefore, the primary goal of this paper is to develop and implement a simple and efficient controller that can handle unpredictable atmospheric conditions and overcome the shortcoming of both conventional and advanced MPPT controllers.

1.2 Status quo on MPPT algorithms in PV systems

There has been much work on developing MPPT approaches to enhance the responsiveness of PV systems. We examine some of these in the following. To enhance a PV system's tracking ability in a wide variety of climates, a fuzzy aided integer order proportional integral derivative with filter (FPIDN)-MPPT approach is proposed. Both temperature and irradiance are fed as input parameters for the FLC. A two-block approach is presented for implementing the MPPT technique. Each MPP's reference voltage is calculated by an adaptive block, while the controller controls the duty cycle. According to the results, the proposed technique outperforms adaptive FLC, P&O, FLC and INC under seven different states of radiation and temperature conditions. The efficiency is measured between 99.45 and 99.72%, and it takes 0.048 s to reach MPP. However, frequent optimization is required for this controller, and it comes at a very high cost [14]. An improved approach, i.e., steady output and fast tracking-MPPT (SOFT) is derived from the INC and P&O algorithms. This approach is tested under constant weather scenarios because its major purpose is to guarantee faster tracking of MPP under fluctuations of radiation and/or temperature, and to give a constant power output. By reducing power losses, the technique improves efficiency over the INC and P&O methods. Although the proposed algorithm has been proven to be more efficient and capable of handling a wide range of loads through simulation and experimentation, it is assessed only in uniform weather conditions, and PSC's effect is not considered [15].

For a stand-alone PV system equipped with a single-ended primary-inductance converter (SEPIC), a load voltage based MPPT (LVB) method is presented. Instead of using a fixed step-size in classical MPPT methods, the suggested method uses adaptive step-size to improve tracking time. Under varied radiation conditions, the proposed control scheme outperforms the fixed step size schemes in the INC and P&O approaches in terms of convergence speed. Moreover, the suggested scheme's resilience is tested under fluctuating load, temperature and PSC circumstances [16]. An enhanced sliding mode controller (SMC) is developed to monitor the optimal MPP position regardless of changes in the sun inclination or the surrounding temperature. The traditional SMC chattering problem is addressed in the suggested method by taking into account the hysteresis quantized input (QI). When compared to traditional SMC, the QI-SMC approach effectively eliminates the chattering and external disturbances from the system. However, the QI-SMC performance is assessed only in uniform weather conditions, and PSC's effect is not considered [17]. A reduced oscillation P&O (ROP&O) technique is implemented to eliminate the oscillation, and decrease the risk of tracking direction loss when PV is exposed to periodic fluctuations in irradiance. The simulation outcome of the RP&O technique is compared with INC and P&O in aspects of ripple, efficiency, tracking time, and error rates. The proposed approach has an efficiency range of 99.06–99.80%, while the MPP can be captured in about 0.018 s, which is 15 times quicker than INC and 5 times faster than P&O. Also, the performance of the ROP&O is verified using a three-phase grid integration condition. Nonetheless, the controller efficacy is not tested in PSC, simultaneously changing load, temperature and radiation conditions [7].

A simple coarse and fine control redesigned P&O method is proposed to maintain simplicity. Besides being simple, the new algorithm overcomes all the issues in the classic P&O, such as slow tracking time, low efficiency, higher oscillation, and power loss. This algorithm contains three distinct control modes, with quick convergence aided by modes 1 and 2, with oscillations in the steady state being kept under control by mode 3. The simulation analysis shows that the suggested approach provides faster tracking time, lower state oscillation, minimal power loss, and improved tracking efficiency compared to drift-free and classical P&O techniques. However, the controller's performance under PSC is not discussed [18]. Complete design of an adaptive robust fuzzy proportional-integral (ARFPI) controller is explored for efficient MPPT of PV system. Steady-state ripple and undershoot are used to evaluate the ARFPI performance under varying temperature and irradiation. In addition, it is compared to classic MPPT techniques, such as INC, PID controller, and P&O to assess its performance. The results show that the ARFPI controller is better (with lower undershoot and ripple), so it can be used as an MPPT controller for PV system [19]. An MPPT approach known as adaptive variable step backstepping (VS-BS) is proposed to enhance the PV system performance. The introduced framework is a hybrid of two MPPT techniques: the nonlinear BS controller and the VS-PO approach. The idea behind the combination of the two separate MPPT methods is to improve tracking speed and accuracy while keeping the scheme simple. The VS-BS approach can capture MPP accurately with no overshoot and negligible ripple under load, temperature, and radiation conditions. However, the efficacy of the proposed controller under PSC is not discussed [20].

To solve the partial shading problem, a new flower pollination-based MPPT approach is implemented. An efficient iterative termination technique is suggested to mitigate the power oscillation once the system has stabilised. The proposed MPPT technique outperforms two well-known techniques, i.e., PSO and P&O, in simulations, demonstrating its ability to quickly and precisely follow GMPP under PSC. However, the proposed technique's efficacy is tested under changing radiation only, while the shading losses under PSC are not discussed [21]. MPPT based on Markov decision process (MDP) is developed for monitoring MPP while it is subjected to the unavoidable occurrence of PSC. Existing approaches, i.e., INC and dynamic leader based MPPT techniques, are analysed and compared to the new method to determine its efficacy. In contrast to conventional methods, which do not account for shading uncertainty, the simulation outcome of MDP reveals a significantly higher maximum power. However, determining the optimal policy requires a high level of computing complexity [22]. An adaptive FLC (AFLC)-MPPT method is presented under four different PSCs. AFLC uses the grey wolf optimization method to improve the membership functions (MFs), therefore yielding the best duty cycle for MPPT. The efficacy and reliability of the AFLC are verified and compared with FLC and P&O on the MATLAB/Simulink platform. It shows that the AFLC not only improves tracking efficiency and speed, but also tracks GMPP in all considered shading patterns. However, the complexity of the AFLC is high, while its effectiveness is not validated under rapidly fluctuating load, radiation and temperature conditions [9].

The PS-FW approach is implemented to address the limitations of both the fireworks algorithm (FWA) and PSO in resolving the GMPPT problem in PSC. Experimental setup and simulation are used to validate the PS-FW approach's efficacy in the GMPPT application over four distinct PSCs. The supremacy of the PS-FW technique is further validated via comparisons of the accuracy and tracking speed of the FWA and PSO methods. Simulation results show that, for one starting population setting, the suggested algorithm improves the GMPP tracking speed by at least 18.51%, while experimental assessment shows that the PS-FW can outperform the GMPP in terms of tracking speed in two different starting population configurations by a margin of at least 23.45%. However, the algorithm's complexity and computational burden are its main drawbacks [23]. For effective MPP accomplishment, a FLC based on an improved bat algorithm (IBA) is presented. For the purpose of tuning the FLC's MFs, IBA is used. The approach can be used to deal with the randomness in irradiance, temperature and PSC. The advantages of the proposed method over more traditional methods, i.e., P&O, FLC, INC are verified by simulation results in a variety of case studies. The simulation outcomes show that the proposed approach can increase the PV system output power by 2–8% in comparison to the traditional approaches in a variety of temperature and radiation conditions. However, the controller's effectiveness is not evaluated under rapidly varying temperature, radiation, and load profile [24].

1.3 Proposed methodology and main contributions

From the above review, it can be seen that the performance of MPPT controllers has not been rigorously tested in real-world situations that involve PSC and simultaneously variations of temperature, radiation, and load profile. Also, speed of convergence, efficiency, power loss, and actual power output need further improvements. Thus, a new Lyapunov-based rapid and ripple-free MPPT using a robust model reference adaptive controller for solar PV system is designed in this paper. The goal of the proposed research is to devise an LRMRAC control law based on Lyapunov stability theorem for a second-order PV MPPT system to achieve rapid convergence, higher efficiency, ripple free, less oscillation in the steady-state, negligible overshoot and undershoot.

The proposed MPPT methodology is based on a sequential two-level hybrid approach, with the first being an MPPT control block and the second an LRMRAC. The first level is based on the classical P&O approach, which generates a reference voltage for each MPP. This MPP voltage is then used as an updated reference voltage and compared to the varying PV voltage caused by changing radiation, load and temperature. The error between the PV voltage and the updated reference voltage is the input to the LRMRAC controller. The art of the LRMRAC lies in fitting appropriate controller parameters. This is accomplished by identifying appropriate adaptive laws. The error between the reference and plant model is used to fine-tune the proposed controller parameters during adaptation. In addition to ensuring closed-loop stability, the adaptive rules must be able to predict the controller's unknown parameters. The Lyapunov stability theorem is used to achieve this objective. LRMRAC provides a reference signal for a duty cycle of PWM that is fed into the boost converter to ensure the PV panel is always being operated at MPP. MATLAB/Simulink is used for the design and implementation of the proposed LRMRAC controller. Probabilistic assessment studies are carried out using simulation and experimental validation of the proposed controller through various levels of uncertainty. At each level, different scenarios are considered and each scenario is influenced by a real-world situation. The uncertainty frameworks of the proposed controller to examine the system robustness are provided at different levels, i.e., Level-I: Variations of temperature, radiation, and load resistance; Level-II: Partially-shaded conditions; and Level-III: OPAL-RT simulator-based experimental validation. Fast-tracking response, low power fluctuation, minimum loss, lower overshoot and undershoot are the key advantages of the proposed MPPT approach. The main contributions of this research are listed below.

1. For the first time, a new LRMRAC controller is proposed for a PV system to achieve efficient MPPT with simple design, easy implementation, higher accuracy and fast convergence.
2. The probabilistic assessment is carried out through three levels of uncertainty to verify the robustness of the proposed controller. The performance of the proposed LRMRAC scheme is compared with classical and advanced MPPT techniques, including P&O, VSPO, INC, and ANFIS.
3. Level 1 uncertainty: At this level, the robustness of the proposed approach is tested in three scenarios, i.e., simultaneously varying load, temperature and radiation profiles, varying both radiation and temperature, and with a slow variation.
4. Seven different load, temperature and radiation states are considered under rapidly varying environmental conditions. The detailed performance comparison of the five algorithms with the seven states is discussed in terms of convergence time, average power output, tracking efficiency, average actual power, overall efficiency, current and voltage ripple, error rates at finding MPP and time domain parameters.
5. The proposed LRMRAC-MPPT approach convergence time is 3.8 ms, power loss is 0.62% and tracking efficiency is between 99.07 and 99.96% under simultaneously varying load, temperature and radiation profiles.
6. Level 2 uncertainty: At this level, the robustness of the proposed approach is tested and compared with P&O and ANFIS in four different partial shading conditions, i.e., Pattern 1: 1000, 1000, 1000 W/m^2; Pattern 2: 500, 400, 700 W/m^2; Pattern 3: 100, 100, 200 W/m^2; and Pattern 4: 1000, 700, 500 W/m^2.
7. The proposed approach harvests the maximum power with negligible oscillation near GMPP. This provides minimal shading losses in all four PSCs.
8. Level 3 uncertainty: At this level, the practicality of the proposed method is demonstrated through experimental validation using the OPAL-RT real-time simulator (OP-4510) at varying temperature and radiation.

A structured methodology is presented in Fig. 1 based on the aforementioned concept to achieve the robust MPPT controller for the PV system. Section 2 depicts the PV system modelling process, and Sect. 3 explains the background and system description. Section 4 provides a concise introduction to the algorithms that are used for comparison, while Sect. 5 provides the detailed methodology of the proposed controller. The findings and analysis from the different levels of uncertainty are presented in Sects. 6 and 7 concludes and summarizes the paper.

2 PV model

A PV cell can be portrayed as a current source connected with a diode, a shunt (R_{pe}) and a series resistance (R_{se}), as depicted in Fig. 2. The single-diode PV model is extensively used since it has fewer parameters and equations than the more complex two-diode model. Hence, a single-diode model is chosen for this study and its mathematical equations are provided as [25]:

$$i_{pv} = I_L - I_s\left[exp\left(\frac{i_{pv}R_{se} + v_{pv}}{V_T}\right) - 1\right] - \left[\frac{i_{pv}R_{se} + v_{pv}}{R_{pe}}\right] \tag{1}$$

where i_{pv} and v_{pv} denote the PV array output current and terminal voltage, respectively. The saturation current is I_s, and V_T is the thermal voltage and is expressed as:

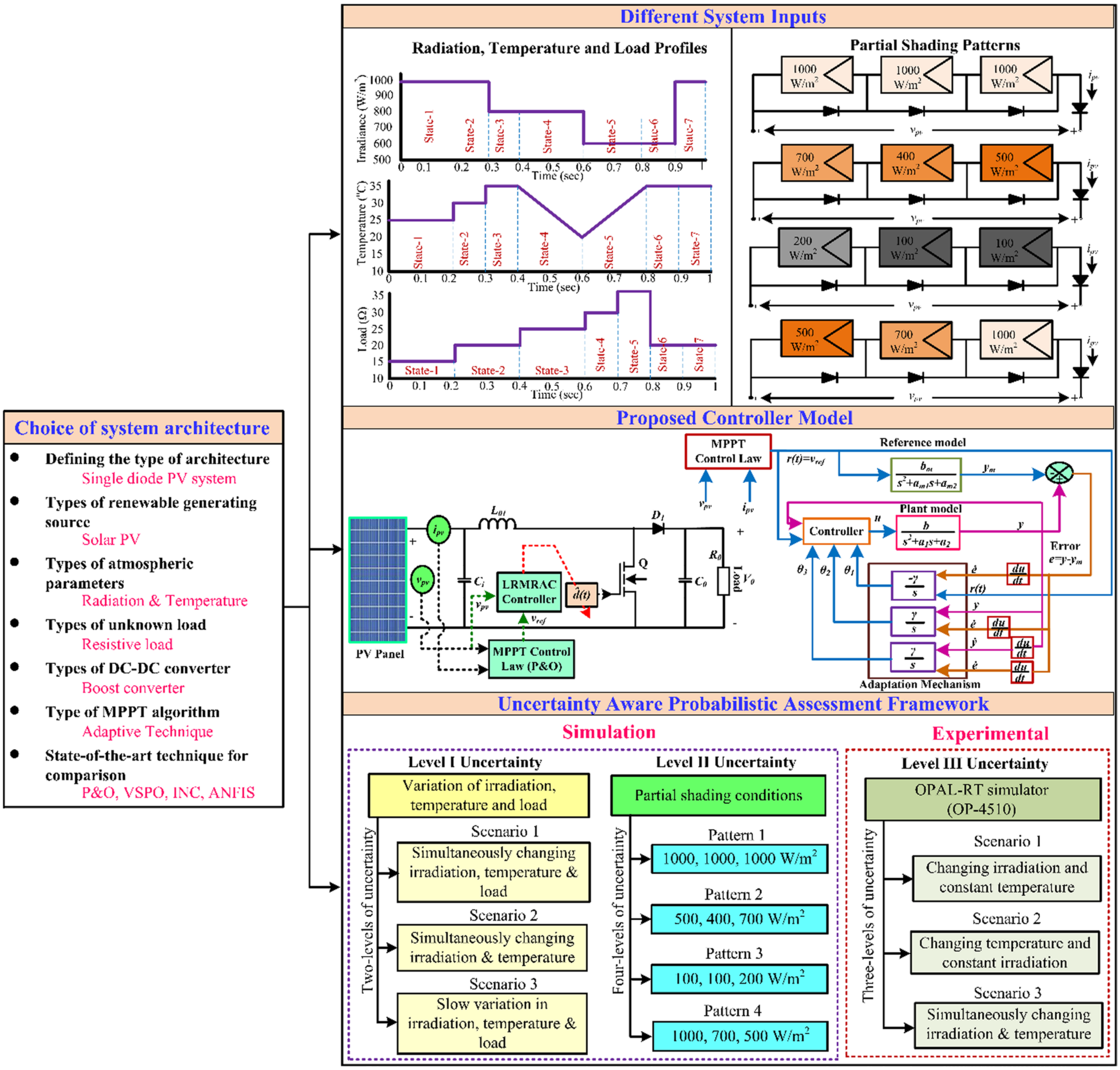

Fig. 1 Graphical representation of structured methodology for the proposed MPPT technique

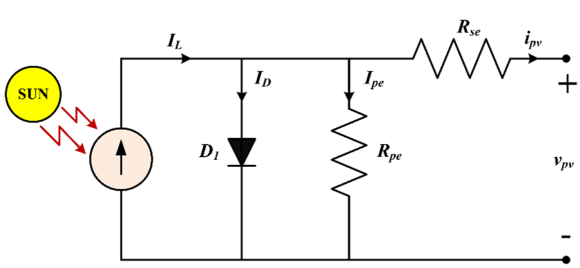

Fig. 2 Electrical equivalent circuit of a PV cell

$$V_T = \left[\frac{nTKN_s}{q}\right] \tag{2}$$

where q is the electron charge. T, K, and n denote temperature, Boltzmann constant, and ideality factor of the diode, respectively. N_s represents the number of cells in a panel that are connected in series.

The PV current is related to irradiance and temperature, as:

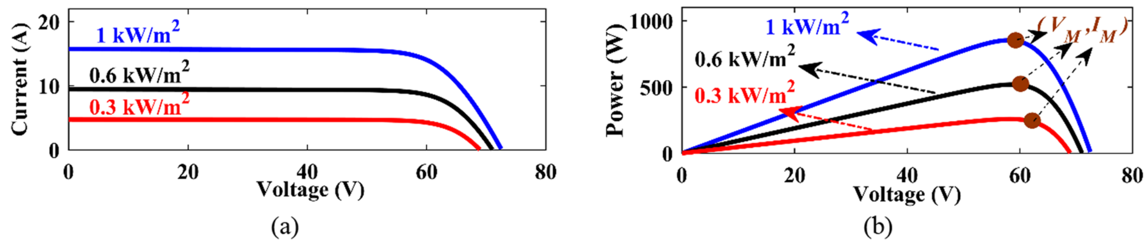

Fig. 3 Solar cell **a** I-V **b** P–V characteristics under variable irradiance (W/m^2)

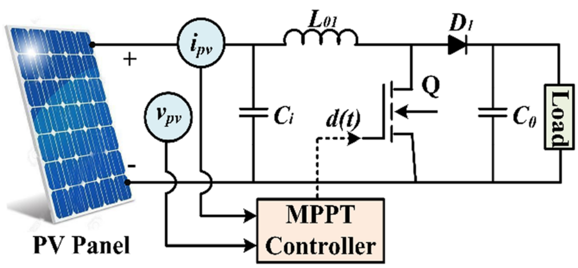

Fig. 4 PV boost converter system with MPPT controller

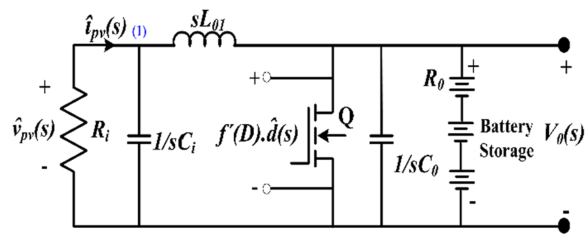

Fig. 5 PV power conversion system's small signal equivalent circuit

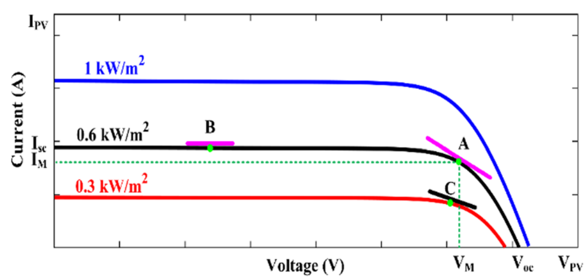

Fig. 6 I-V characteristics with changing R_i superimposed over the graph

$$I_L = I_L(G)[1 + K_t(T - T_a)] \quad (3)$$

$$I_L(G) = I\left(\frac{G}{G_{st}}\right) \quad (4)$$

where T_a and T represent ambient absolute and standard temperatures, respectively. I_L denotes photocurrent and K_t is temperature coefficient at 1000 W/m^2 and 25 °C. Here, G_{st} = standard irradiance and G = irradiance (W/m^2).

This research uses the "1Soltech 1STH-215-P" solar module. Environmental conditions affect the electrical properties of PV arrays. Figure 3 illustrates simulated I–V and P–V characteristics of the PV array at constant temperature (25 °C) and under various radiation conditions ranging from 0.3 to 1 kW/m^2.

As can be observed in Fig. 3, the MPP occurs when the rate of change of power to the voltage is zero. This is represented mathematically by:

$$\frac{dp}{dv_{pv}}\left\{\begin{array}{l} = 0,\ at\ the\ MPP \\ < 0,\ at\ the\ right\ side\ of\ the\ MPP \\ > 0,\ at\ the\ left\ side\ of\ the\ MPP \end{array}\right\} \quad (5)$$

3 Background and system description

3.1 MPPT concept in PV system

Figure 3a depicts the PV system's I-V curve at various solar radiation levels. At the "knee" of the I–V curve (I_M, V_M), MPP occurs, and the maximum power (P_M) is achieved when either I_M or V_M is obtained.

Figure 4 depicts a basic PV system with a solar panel and a dc-dc converter that is interfaced with an MPPT controller to maximise power output. The MPPT controller converts the measured voltage (v_{pv}) and current (i_{pv}) from the PV panels into a duty cycle (d) in order to manage the switch Q. This PV array's current and voltage are composed of ripple and DC components. The MPPT scheme's purpose is to extract maximum power so that i_{pv} and v_{pv} follows I_M and V_M as depicted in Figs. 3 and 6.

The steady-state relationship between i_{pv}, v_{pv}, and d of the switch Q can be stated as:

$$v_{pv} = i_{pv}R_0(1 - d)^2 \quad (6)$$

with $v_{pv} = V_{pv} + \widehat{v}_{pv}$ and $i_{pv} = I_{pv} + \widehat{i}_{pv}$. I_{pv} & $\widehat{i}_{pv}$ are the PV array DC and ripple currents, respectively, whereas V_{pv} and $\widehat{v}_{pv}$ are respectively the PV array DC and ripple voltages.

3.2 PV system small-signal modeling with power-conversion stage

Equation (6) shows the steady-state relationship between the converter duty cycle and array voltage. The dynamics between array voltage and duty cycle must be considered in MPPT control to optimise the transient response. Figure 5 depicts a small signal equivalent to the circuit in Fig. 4 to simplify the transient response analysis [26]. $\widehat{i}_{pv}(s)$, $\widehat{v}_{pv}(s)$ and R_i represent the small signal (SS) PV array current, voltage and resistance, respectively, as shown in Fig. 5. The transfer function from $\widehat{v}_{pv}(s)$ to $\widehat{d}(s)$ in small signal operation is now developed around an operational point, ignoring the battery load. At node (1), using the KCL method, the relationship between $\widehat{v}_{pv}(s)$ and $\widehat{d}(s)$ is determined in the frequency domain as [27]:

$$\frac{\widehat{v}_{pv}(s)}{R_i} + s\widehat{v}_{pv}(s)C_i = \frac{f^{'}(D)\widehat{d}(s) - \widehat{v}_{pv}(s)}{sL_{01}} \tag{7}$$

where $\widehat{d}$ denotes the SS variation around the duty cycle D at the operating point, $\widehat{v}_{pv}(s)$ and $\widehat{d}(s)$ are the Laplace transforms of $\widehat{v}_{pv}(t)$ and $\widehat{d}(t)$, respectively. $f(D)$ represents the correlation between the boost converter steady-state DC input voltage (V_{pv}) and the operating duty cycle (D). At operating point D, $f'(D)$ is the derivative of $f(D)$ with regard to the duty cycle.

Rearranging (7) yields:

$$\frac{\widehat{v}_{pv}(s)}{\widehat{d}(s)} = \frac{f^{'}(D)}{L_{01}C_i s^2 + \frac{L_{01}}{R_i}s + 1} \tag{8}$$

It is well-known that:

$$f(D) = V_{pv} = (1 - D)V_0 \tag{9}$$

where V_0 is the boost converter steady state DC output voltage. The DC steady state relationship between V_0 and $f(D)$ is assumed to be unaffected by the transient action in (9). Thus, with respect to (9), there is:

$$f^{'}(D) = -V_0 \tag{10}$$

Substituting $f'(D)$ value from (10) into (8) yields:

$$\frac{\widehat{v}_{pv}(s)}{\widehat{d}(s)} = \frac{-\frac{V_0}{L_{01}C_i}}{s^2 + \frac{1}{R_iC_i}s + \frac{1}{L_{01}C_i}} \tag{11}$$

According to (11), the panel voltage will increase if the duty ratio decreases as implied by the negative sign. Figure 5 depicts the linearized representation of the nonlinear system seen in Fig. 4 at a single operational point, from which the aforementioned transfer function was calculated. The system operating point changes when the amount of solar insolation changes, resulting in a change in the effective values of (11), particularly R_i. The denominator of (11) can be analysed in canonical form to show the impact of R_i on the system, i.e.:

$$s^2 + 2\xi\omega_n s + \omega_n^2 \tag{12}$$

where ξ and ω_n represent the damping ratio and natural frequency, respectively. Comparing the denominators of (11) and (12) yields:

$$\xi = \frac{1}{2R_i}\sqrt{\frac{L_{01}}{C_i}} \text{ and } \omega_n = \frac{1}{\sqrt{L_{01}C_i}}$$

In systems with ξ <1, oscillation can be seen in the step response because the system is underdamped. Controlling the plant with an adaptive controller is one method of preventing under-damped oscillation and other undesirable behaviour. Ideally, ξ should approach one such that the system is critically damped (CDS). It is possible to alter the value of R_i to achieve CDS at a single operating point, but it is impossible to maintain CDS at all operating points with fixed R_i.

At the three distinct solar insolations, i.e., 0.3, 0.6, and 1 kW/m^2, the I–V characteristics of the PV array are illustrated again in Fig. 6. The slope tangential to the system's operating point can be used to calculate the PV array's R_i value, i.e.:

$$\frac{1}{R_i} \approx -\frac{\Delta I}{\Delta V} \tag{13}$$

Figure 6 illustrates the MPP for the 0.6 kW/m^2 curves, indicated by the letter A with V_M and I_M. According to (13), one can determine the R_i value at point A by measuring the inverse slope's magnitude on the line tangential to the location A. It is clear that the value of R_i will change if the operational point is moved from A to B while maintaining constant solar insolation. In addition, a different value of R_i is produced when moving the operational point from A to C, which is the MPP for 0.3 kW/m^2 solar radiation. Thus, it is impossible to ensure that if the MPP switches, the operational R_i will remain unchanged. Furthermore, it is not guaranteed that the operational optimal R_i will result in CDS. As a result, a new LRMRAC technique is proposed in this study to track MPP. The proposed method can effectively achieve CDS (ξ=1) while also forcing the operating point to be optimal R_i and optimising the converter dynamics.

4 MPPT techniques

This section provides a concise introduction to the algorithms that are used for comparison. The parameter settings of the INC [6] and P&O [7] algorithms used in this study have been explained in the literature, so only the ANFIS and VSPO techniques are briefly explained below.

4.1 VSPO

In order to address the shortcomings of the standard fixed-step-size P&O approach, a variable-step P&O (VSPO) method is implemented. The VSPO method has two distinct step size increments which are changeable. The approach uses the current variation (di_{pv}) to choose between these two steps for MPPT. Thus, an increase in di_{pv} is a result of an increase in the level of solar irradiation, since increased irradiation produces an increased current. Thereby, the size of each subsequent step increases, which is accomplished by using (14). However, if the solar irradiance level drops, the current also drops, resulting in a smaller step size, and therefore, (15) is used instead. The flowchart is shown in Fig. 7 [28].

$$Step1 = \left(\frac{N}{i_{pv}}\left|\frac{dp}{dv_{pv}}\right|\right)A_1 \tag{14}$$

$$Step2 = \left(\frac{N}{i_{pv}}\left|\frac{dp}{dv_{pv}}\right|\right)A_2 \tag{15}$$

where N is the scale factor, A_1 and A_2 are the normalization coefficients with $A_1 < 1 < A_2$. Here, N, A_1 and A_2 are taken as 0.001, 0.5 and 10, respectively.

4.2 ANFIS

ANFIS is a type of adaptive network that takes on the characteristics of a fuzzy and neural inference system. The adaptive network is devoid of synaptic weights but contains both non-adaptive and adaptive nodes. The term "adaptive network" refers to the straightforward transformation into a neural network structure employing a standard feedforward topology.

ANFIS is an adaptive network which acts like the adaptive network simulator of Takagi–Sugeno's fuzzy controllers, and its operation resembles that of a fuzzy inference system (FIS). ANFIS adapts its output and input parameters using least-squares and back-propagation gradient descent for the specified output/input data. ANFIS has

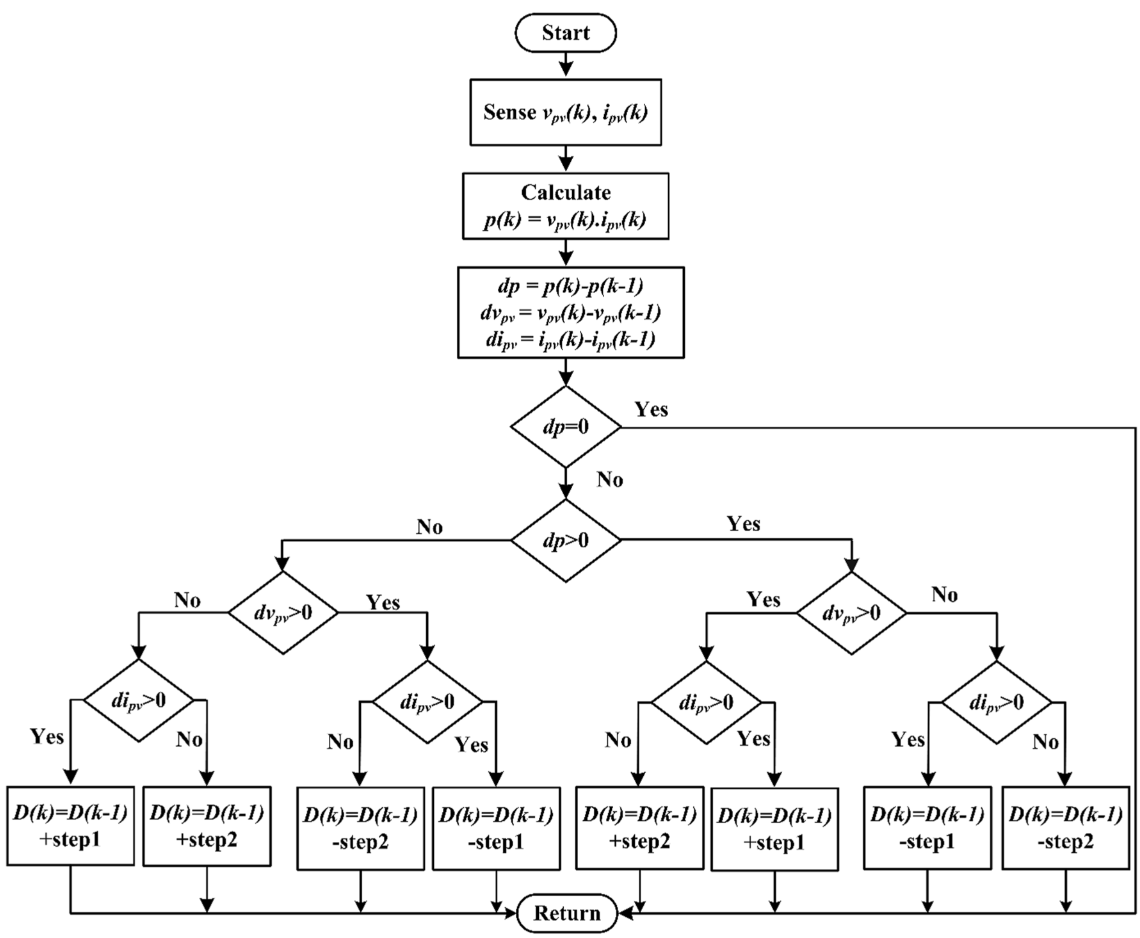

Fig. 7 Flowchart of VSPO algorithm

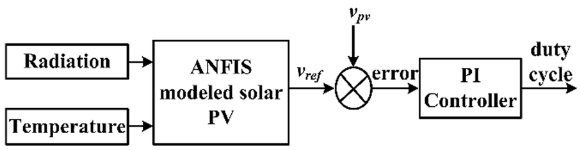

Fig. 8 Block diagram of ANFIS-MPPT

two parts, i.e., the antecedent part and consequent part that are connected by rule-based FIS [29].

When ANFIS is being trained, it takes in data about temperature and radiation, and produces a single output of voltage, at varying levels of temperature and radiation. The ANFIS output is used as a reference voltage, which is then compared to the actual PV voltage to generate an error. The obtained error is handled by a PI controller to be turned into the duty cycle. For optimal power harvesting from a solar PV array, a PWM generator provides the pulse for the DC–DC converter. The overall block diagram of ANFIS-MPPT is displayed in Fig. 8, and the parameters used in ANFIS-MPPT are given in Table 1.

5 Proposed MPPT methodology

An MPPT control law (P&O) unit serves as the first level of control in the proposed MPPT method, as depicted in Fig. 9. A reference voltage (v_{ref}) is generated by this control block for each MPP voltage.

In the second stage, the proposed LRMRAC-MPPT controller is implemented. The PV array and reference voltages are compared, and the obtained error (v_{pv}-v_{ref}) is then fed into the LRMRAC as an input variable. To keep the PV panel working at MPP at all times, the LRMRAC produces a reference signal for the duty cycle of the switch Q.

5.1 MPPT control block (P&O)

An individual reference voltage (v_{ref}) is computed for each MPP voltage by this MPPT control block. A voltage-reference-based P&O approach is developed to implement the MPPT control scheme. Equation (5)

Table 1 Simulation parameters

Parameter	Numerical value	Parameter	Numerical value
Rated current (I_{MPP})	7.35 A	Boost inductor (L_{01})	2 mH
Short-circuit current (I_{sc})	7.84 A	Boost output capacitor (C_0)	100 µF
Rated voltage (V_{MPP})	29 V	Load value (R_0)	20 Ω
Open-circuit voltage (V_{oc})	36.3 V	Output voltage range (V_0)	112.5–129.1 V
Rated power (p_{max})	213.15 W	Input voltage range (V_{IN})	56.6–60.3 V
R_{se}	0.39383 Ω	b_m	5.75×10^8 V(rad/sec)^2
R_{pe}	313.3991 Ω	$b = V_0/L_{01} \times C_i$	6.45×10^8 V(rad/sec)^2
Number of parallel modules	2	a_{m1}	8.17×10^3(rad/sec)
Number of series module	2	$a_1 = 1/R_i \times C_i$	400 (rad/sec)
Cells per module	60	a_{m2}	1.67×10^7(rad/sec)^2
R_i	25 Ω	$a_2 = 1/L_{01} \times C_i$	1.67×10^7(rad/sec)^2
Boost input capacitor (C_i)	100 µF	Adaptation gain (γ)	0.08
Switching frequency (f_s)	20 kHz	Simulation step time (T_s)	1 µsec

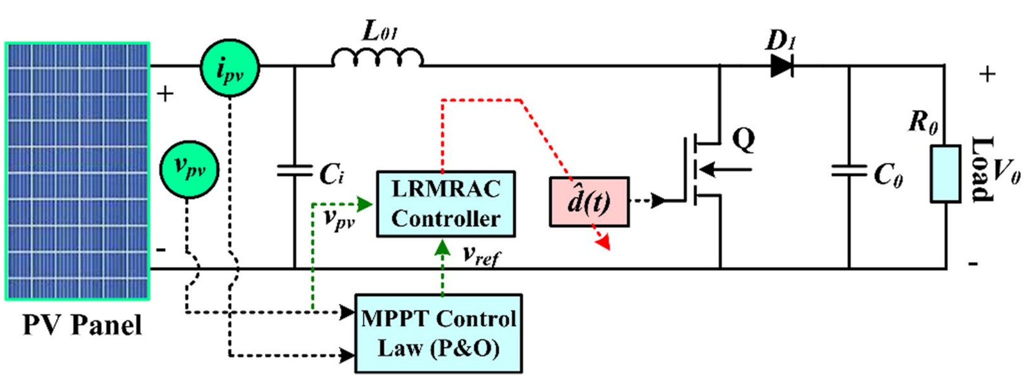

Fig. 9 Representation of the proposed MPPT control architecture for a PV system

refers to the MPPT control law where maximum power occurs, and v_{ref} of the controller can vary according to (16), where Δv and v_{pv} denote a small threshold voltage and PV array voltage respectively.

$$v_{ref} = \begin{cases} v_{pv}, \frac{dp}{dv_{pv}} = 0 \\ v_{pv} - \Delta v, \frac{dp}{dv_{pv}} < 0 \\ v_{pv} + \Delta v, \frac{dp}{dv_{pv}} > 0 \end{cases} \quad (16)$$

Figure 10 depicts the flowchart of the proposed MPPT method for generating the reference voltage.

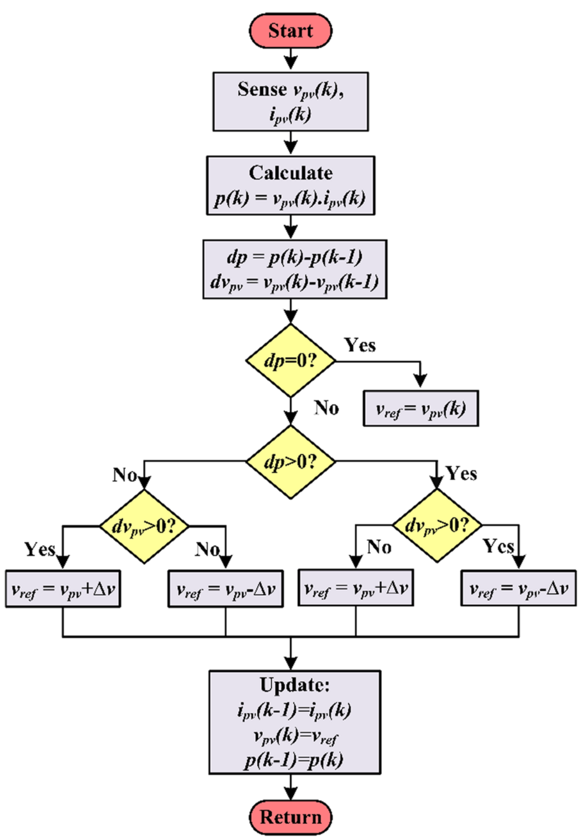

Fig. 10 Flowchart for generating the reference voltage

5.2 Proposed LRMRAC method

In the preceding steps, P&O is used to determine v_{ref}, which seeks to deliver the maximum power available in steady-state conditions. In addition, it is desired that the system converges to MPP when solar insolation changes quickly. From (11), it can be seen that the relationship between the duty cycle and array voltage is a highly dynamic process. Without adaptive control, the array voltage may not display critically damped behaviour because the operating point will fluctuate with changes in solar insolation. The main goal of the LRMRAC design is thus to maintain the array voltage critically damped.

The core concept behind the LRMRAC is the development of an adaptive controller that is independent of uncertainties or variations in plant parameters, so as to ensure the plant response is close to the response of the reference model.

However, most plants, including a PV system with boost converter, are second-order systems. However, traditional MRAC tracking performance for second-order systems is unsatisfactory. The control law for the second order system along with extension from the first to the second order of the LRMRAC is derived here. The proposed LRMRAC architecture is seen in Fig. 11. The v_{ref} determined in Sect. 5.1 serves as the input (*r(t)*) to the entire system. The plant model in Fig. 11 corresponds to the transfer function in (11). However, to keep things straightforward, its sign is flipped so that the plant model has only positive coefficients.

Here, *y(t)* and *u(t)* denote plant output and input, respectively.

The time and frequency domain descriptions of the second order plant model are provided by:

$$\frac{d^2y(t)}{dt^2} = -a_1\frac{dy(t)}{dt} - a_2y(t) + bu(t) \quad (17)$$

$$\frac{y(s)}{u(s)} = \frac{b}{s^2 + a_1s + a_2} \quad (18)$$

The desired responses are presented in time and frequency domains by:

$$\frac{d^2y_m(t)}{dt^2} = -a_{m1}\frac{dy_m(t)}{dt} - a_{m2}y_m(t) + b_mr(t) \quad (19)$$

$$\frac{y_m(s)}{r(s)} = \frac{b_m}{s^2 + a_{m1}s + a_{m2}} \quad (20)$$

where both a_{m1}, $a_{m2}>0$ and the reference signal (*r(t)*) is bounded.

The controller is given as:

$$u = \theta_1 r - \theta_2 y - \theta_3 \dot{y} = \theta^T\varphi \quad (21)$$

where ϕ is defined as $[r, y, \dot{y}]^T$, and $\theta = [\theta_1, \theta_2, \theta_3]^T$ is the controller parameter estimation vector.

Substituting (21) into (17) yields:

$$\frac{d^2y(t)}{dt^2} = -(a_1 + b\theta_3)\frac{dy(t)}{dt} - (a_2 + b\theta_2)y(t) + b\theta_1 r(t) \quad (22)$$

Comparing the coefficients in (19) and (22) yields:

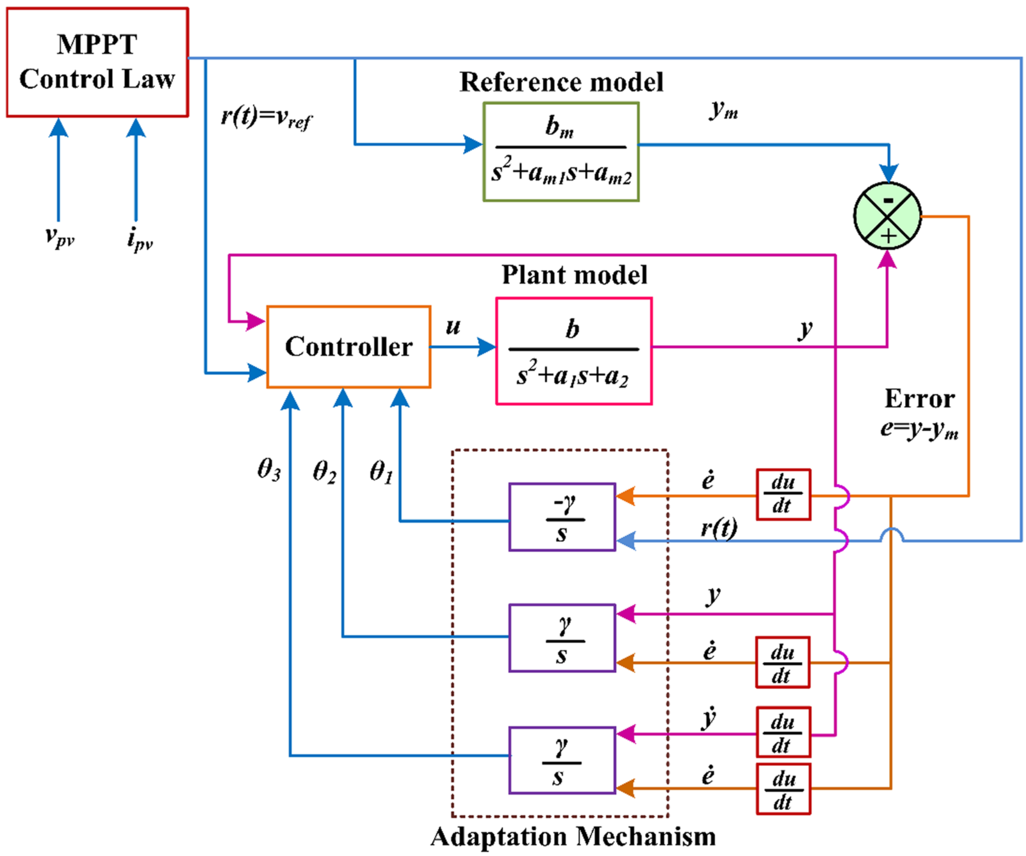

Fig. 11 Controller structure in the proposed LRMRAC

$$b\theta_1 = b_m \tag{23}$$

$$a_{m2} = a_2 + b\theta_2 \tag{24}$$

$$a_{m1} = a_1 + b\theta_3 \tag{25}$$

where θ_1, θ_2, and θ_3 are the control parameters that are converged as:

$$\theta_1 \approx \frac{b_m}{b}; \theta_2 \approx \frac{a_{m2}-a_2}{b}; \theta_3 \approx \frac{a_{m1}-a_1}{b} \tag{26}$$

Introduce the error as:

$$e = y - y_m \tag{27}$$

Since it seeks to minimise the error, it is reasonable to derive a differential equation for the error.

Taking the first and second derivatives of the error equation in (27):

$$\frac{de}{dt} = \frac{dy}{dt} - \frac{dy_m}{dt} \tag{28}$$

$$\frac{d^2e}{dt^2} = \frac{d^2y}{dt^2} - \frac{d^2y_m}{dt^2} \tag{29}$$

Substituting (17) and (19) into (29) and replacing u as in (21) result in:

$$\begin{aligned}\frac{d^2e}{dt^2} =& \frac{dy}{dt}(-a_1 - b\theta_3 + a_{m1}) + y(-a_2 - b\theta_2 + a_{m2}) \\ &+ r(b\theta_1 - b_m) - a_{m1}\frac{de}{dt} - a_{m2}e\end{aligned} \tag{30}$$

If the parameter values are equal to the values in (26), $e(t)$ becomes zero. To get the appropriate or desired θ_1, θ_2 and θ_3 parameter values, a parameter adjustment mechanism is designed. As per Lyapunov stability theorem, if there exists a scalar function $V(t)$ which is real, continuous, and has continuous first partial derivatives with $\dot{V}(t) < 0$ for all $t \neq 0$, then the system is asymptotically stable.

Assume $b\gamma > 0$ and define the Lyapunov function V for this purpose as:

$$V(e,\dot{e},\theta_1,\theta_2,\theta_3) = \frac{1}{2}\frac{(a_1+b\theta_3-a_{m1})^2}{b\gamma} + \frac{1}{2}\frac{(a_2+b\theta_2-a_{m2})^2}{b\gamma} + \frac{1}{2}\frac{(b\theta_1-b_m)^2}{b\gamma} + \frac{1}{2}\left(\frac{de}{dt}\right)^2 + \frac{1}{2}a_{m2}e^2 \tag{31}$$

For this function, $V=0$ when $e=0$, and the controller parameters, i.e., θ_1, θ_2, θ_3 are equal to the correct values. When dV/dt is negative, the function is a Lyapunov one. The derivative is given as:

$$\frac{dV}{dt} = \frac{(a_1+b\theta_3-a_{m1})}{\gamma}\left(\frac{d\theta_3}{dt}-\dot{e}\dot{y}\right) + \frac{(a_2+b\theta_2-a_{m2})}{\gamma}\left(\frac{d\theta_2}{dt}-\dot{e}y\right) + \frac{(b\theta_1-b_m)}{\gamma}\left(\frac{d\theta_1}{dt}+\dot{e}r\right) - a_{m1}\dot{e}^2 \tag{32}$$

If the parameters are updated as:

$$\frac{d\theta_1}{dt} = -\gamma r\dot{e} \tag{33}$$

$$\frac{d\theta_2}{dt} = \gamma y\dot{e} \tag{34}$$

$$\frac{d\theta_3}{dt} = \gamma \dot{y}\dot{e} \tag{35}$$

there is:

$$\frac{dV}{dt} = -a_{m1}\dot{e}^2 \tag{36}$$

Thus, the time derivative of V is negative semidefinite rather than negative definite. Therefore, it implies $V(t) \le V(0)$ and thus, e, $\dot{e}$, θ_1, θ_2, and θ_3 must be bounded. This concludes that $y = e + y_m$ is also bounded. Now a necessary condition to prove is $\ddot{V}$ bounded. $\ddot{V}$ is given as:

$$\frac{d^2V}{dt^2} = -2a_{m1}\dot{e}\frac{d\dot{e}}{dt} = -2a_{m1}\dot{e}\left\{\begin{array}{c} -\frac{dy}{dt}(a_1+b\theta_3-a_{m1}) \\ -y(a_2+b\theta_2-a_{m2})+r(b\theta_1-b_m) \\ -a_{m1}\frac{de}{dt}-a_{m2}e \end{array}\right\}$$

Since r, e, and y are bounded, it follows that $\ddot{V}$ is also bounded. Hence, dV/dt is uniformly continuous. Equations (33), (34), and (35) are the adaptation rule.

6 Results and discussion

MATLAB/SIMULINK is used to design the proposed LRMRAC-MPPT controller. The three primary components of the simulation are the PV model, the boost converter model, and the adaptive controller. The proposed MPPT technique is compared to other well-known techniques such as P&O, VSPO, INC, and ANFIS. Different uncertainties are identified and probabilistic assessments are carried out at three levels. Both simulation and experimental studies are undertaken to validate the system robustness under diverse atmospheric conditions. Table 1 lists all the simulation parameters for the proposed system. The MPPT scheme tracking efficiency (η) is calculated as [20]:

$$\eta = \frac{\int_{t_1}^{t_2} p_{avg}dt}{\int_{t_1}^{t_2} p_{max}dt} \tag{37}$$

The algorithm begins tracking at moment t_1 and ends at time t_2. The average power produced between t_1 and t_2 is denoted by p_{avg}, and the theoretical maximum power available is denoted by p_{max}. The current and voltage ripples refer to the corresponding peak-to-peak values. The following equations are used to calculate the errors of the five different techniques and n is defined as the number of data points.

RMSE (Root mean square error)

$$= \sqrt{\frac{\sum (ActualValue - EstimatedValue)^2}{n}} \tag{38}$$

MAE (Mean absolute error

$$= \frac{\sum |EstimtedValue - ActualValue|}{n} \tag{39}$$

MAPE (Mean absolute percentage error)

$$= \frac{1}{n}\sum\left(\frac{|Actual - Forecasting|}{|Actual|}\right) \times 100\% \tag{40}$$

6.1 Level-I uncertainty

6.1.1 Simultaneously changing load, temperature and radiation

Figures 12a, b and c show the variations in radiation, temperature, and load signal. There are seven possible states for each signal. State 1 is 1 kW/m^2, 25 °C, 15Ω, State 2 is 1 kW/m^2, 30 °C, 20Ω, etc. The PV system with changing load resistance causes unpredictable disturbances in the system. Figure 13 shows the PV array power for the five different MPPT approaches (LRMRAC, ANFIS, VSPO, INC and P&O) as the load, temperature and radiation all change

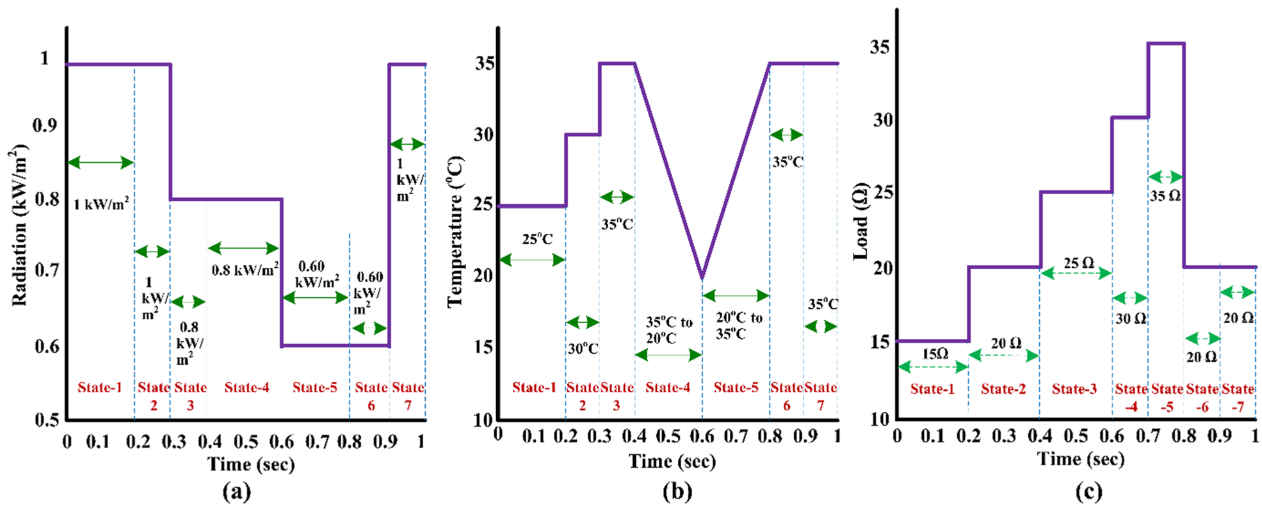

Fig. 12 **a** Radiation **b** Temperature **c** Load profile

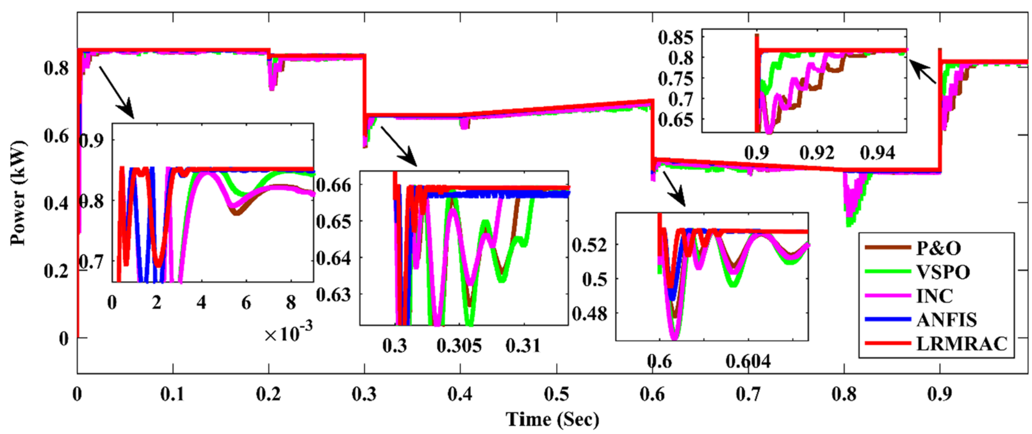

Fig. 13 PV power using the five MPPT algorithms while temperature, irradiance, and load all change at once

at the same time. The ripple around the MPP is the highest for the INC, VSPO, and P&O methods, but is reduced for the ANFIS method though at the expense of not being able to achieve MPP. The proposed method has almost no ripple near the MPP across all seven states. Table 2 clearly indicates that the proposed controller has, compared to other methods, lower voltage and current ripples, higher output power, less convergence time, higher tracking and overall efficiency, and less error finding the MPP in all seven states.

The relative speeds of the various MPPT methods are shown in Fig. 14. The novel MPPT approach captures MPP in 0.0038 s, compared to 0.021 s for ANFIS, 0.16 s for VSPO, 0.20 s for INC, and 0.20 s for P&O. Thus, the proposed MPPT method is the quickest at acquiring MPP.

Comparative graphical representations of convergence time, tracking efficiency, tracking power loss, voltage and current ripples for all the five MPPT approaches under the seven different states are illustrated in Figs. 15 (a)-(d), respectively. The power loss (p_{loss}) is measured by [7]:

$$p_{loss} = \frac{\sum p_{max}(t) - \sum p_{pv}(t)}{\sum p_{max}(t)} \tag{41}$$

where the actual power is denoted by p_{pv}, and $p_{max} = p_{mpp}$ is the maximum power. t relates to the tracking time required by various MPPT methods in order to reach MPP. As shown in Fig. 15(c), as compared to ANFIS, INC, VSPO and P&O schemes, the proposed MPPT approach generates the lowest power loss. This means that the proposed technique completely eliminates oscillations and achieves the highest tracking efficacy in all states.

Table 2 Detail comparative analysis of the five approaches with 7 states

MPPT Techniques	State 1	State 2	State 3	State 4	State 5	State 6	State 7
Voltage ripple (V)							
P&O	3.07	3.94	3.57	4.81	4.70	3.88	1.90
VSPO	2.60	3.42	3.27	4.61	4.04	2.70	1.10
INC	2.96	3.93	3.56	4.58	4.50	4.05	1.50
ANFIS	1.00	0.2	0.41	0.31	0.52	1.47	0.03
LRMRAC	0.1	0.13	0.016	0.093	0.068	0.50	0.02
Current ripple (A)							
P&O	0.84	1.08	0.86	1.03	0.96	0.70	0.73
VSPO	0.66	0.95	0.69	1.01	0.71	0.67	0.40
INC	0.81	1.08	0.85	1.03	0.84	0.71	0.70
ANFIS	0.23	0.056	0.04	0.034	0.061	0.063	0.007
LRMRAC	0.028	0.037	0.022	0.022	0.015	0.028	0.004
Power loss (%)							
P&O	3.50	2.56	3.77	2.46	2.78	3.40	4.19
VSPO	2.98	2.48	3.63	2.33	2.50	3.07	4.10
INC	3.50	2.55	3.78	2.46	2.78	3.41	4.19
ANFIS	0.62	1.07	2.55	1.53	1.41	2.11	3.14
LRMRAC	0.04	0.07	0.29	0.03	0.50	0.03	0.04
Average actual power (W)							
P&O	822.2	830.1	655.9	664.8	496.9	493.8	816.3
VSPO	826.6	830.8	656.8	665.7	498.4	495.5	817.0
INC	822.2	830.1	655.8	664.8	496.9	493.7	816.3
ANFIS	846.7	842.8	664.2	671.2	503.9	500.4	825.2
LRMRAC	851.7	851.4	679.6	681.2	508.6	511.0	851.6
Average power output (W)							
P&O	815.3	812.6	651.4	648.6	486.2	487.4	815.6
VSPO	824.1	821.1	659.1	659.8	491.3	493.7	823.9
INC	815.3	812.6	651.5	648.5	486.2	487.4	815.6
ANFIS	834.8	833.3	666.0	663.2	496.4	498.8	832.8
LRMRAC	842.5	842.2	668.2	669.9	501.5	505.3	841.8
Convergence time (s)							
P&O	0.20	0.10	0.10	0.20	0.780	0.10	0.089
VSPO	0.16	0.10	0.10	0.19	0.748	0.10	0.065
INC	0.20	0.10	0.10	0.20	0.758	0.10	0.070
ANFIS	0.021	0.0062	0.04	0.07	0.014	0.014	0.0056
LRMRAC	0.0038	0.0053	0.005	0.006	0.0064	0.0081	0.0039
Tracking efficiency (%)							
P&O	97.66	97.44	96.13	97.91	97.81	96.60	96.81
VSPO	98.73	98.46	98.37	98.16	98.81	98.85	98.79
INC	97.66	97.44	97.23	97.91	97.81	97.61	97.81
ANFIS	99.15	99.12	98.85	99.27	99.61	98.79	99.18
LRMRAC	99.96	99.93	99.70	99.78	99.81	99.07	99.88
Overall efficiency (%)							
P&O	95.70	95.38	95.58	95.16	95.11	95.36	95.73
VSPO	96.73	96.38	96.70	96.81	96.11	96.58	96.71
INC	95.70	95.38	95.59	95.15	95.11	95.36	95.73
ANFIS	97.99	97.81	97.72	97.30	97.11	97.59	97.75
LRMRAC	98.89	98.85	98.04	98.29	98.11	98.84	98.81

Table 2 (continued)

MPPT Techniques	State 1	State 2	State 3	State 4	State 5	State 6	State 7
RMSE error							
P&O	0.0039	0.0221	0.0258	0.0172	0.0131	0.0175	0.0361
VSPO	0.0037	0.0220	0.0249	0.0168	0.0121	0.0168	0.0357
INC	0.0039	0.0221	0.0259	0.0172	0.0131	0.0174	0.0361
ANFIS	0.0006	0.0177	0.0234	0.0156	0.0091	0.0159	0.0312
LRMRAC	0.0003	0.0166	0.0215	0.0146	0.0031	0.0140	0.0251
MAE Error							
P&O	0.0031	0.0218	0.0257	0.0172	0.0131	0.0173	0.0357
VSPO	0.0028	0.0218	0.0248	0.0167	0.0121	0.0157	0.0341
INC	0.0031	0.0218	0.0258	0.0171	0.0131	0.0172	0.0357
ANFIS	0.0005	0.0177	0.0233	0.0156	0.0091	0.0149	0.0252
LRMRAC	0.0003	0.0156	0.0124	0.0135	0.0031	0.0120	0.0141
MAPE error (%)							
P&O	0.3591	2.562	3.772	2.519	2.563	3.382	4.193
VSPO	0.3215	2.552	3.644	2.476	2.543	3.079	4.100
INC	0.3610	2.565	3.784	2.516	2.563	3.375	4.188
ANFIS	0.0564	2.076	3.172	2.376	2.163	2.015	3.138
LRMRAC	0.0203	1.052	2.299	1.575	1.568	1.635	2.122

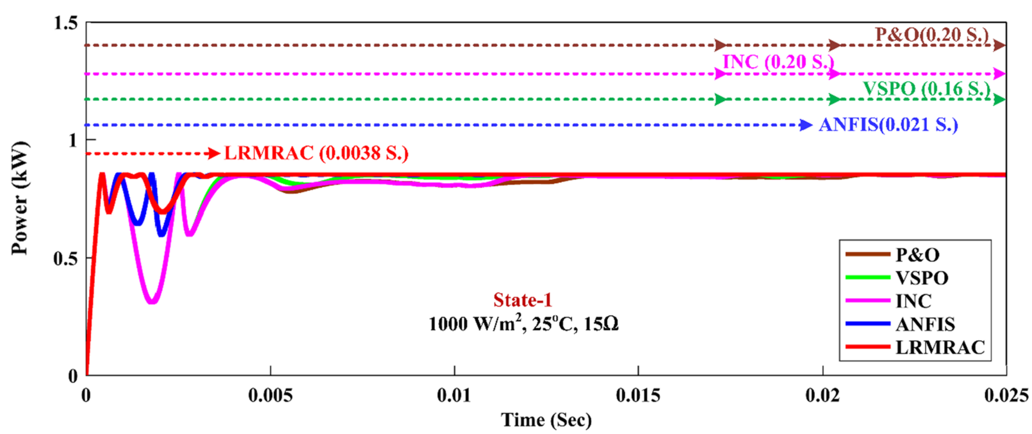

Fig. 14 Speed of the different MPPT algorithms while temperature, irradiance, and load all change at once

6.1.2 Simultaneously changing radiation and temperature

The radiation and temperature patterns are displayed in Figs. 12a and b, respectively. All the states mentioned are based on possible daily changes in environmental conditions. Figure 16 shows the PV array power for the five different MPPT approaches when temperature and irradiation change simultaneously. On the basis of Fig. 17, it can be deduced that P&O takes the longest time to track MPP in 0.1 s, followed by INC in 0.07 s, VSPO in 0.05 s, ANFIS in 0.007 s, while the proposed method takes only 0.0037 s. In all seven states, MPP is rapidly tracked using the LRMRAC technique.

The INC, VSPO and P&O approaches have substantial ripples, while ANFIS has fewer and the proposed technique has negligible ripple. While analyzing the convergence time the values are 0.1 s, 0.043 s, 0.03 s, 0.037 s, 0.016 s, 0.01 s and 0.042 s in states 1–7 respectively for the P&O scheme. In case of INC, convergence times are 0.07 s, 0.034 s, 0.025 s, 0.029 s, 0.015 s, 0.011 s and 0.034 s in states 1–7, respectively. For VSPO, convergence times are 0.05 s, 0.03 s, 0.023 s, 0.026 s, 0.014 s, 0.02 s and 0.015 s in states 1 to 7, respectively. In case of ANFIS convergence times are 0.007 s, 0.004 s, 0.008 s, 0.0089 s, 0.005 s, 0.0042 s and 0.0058 s

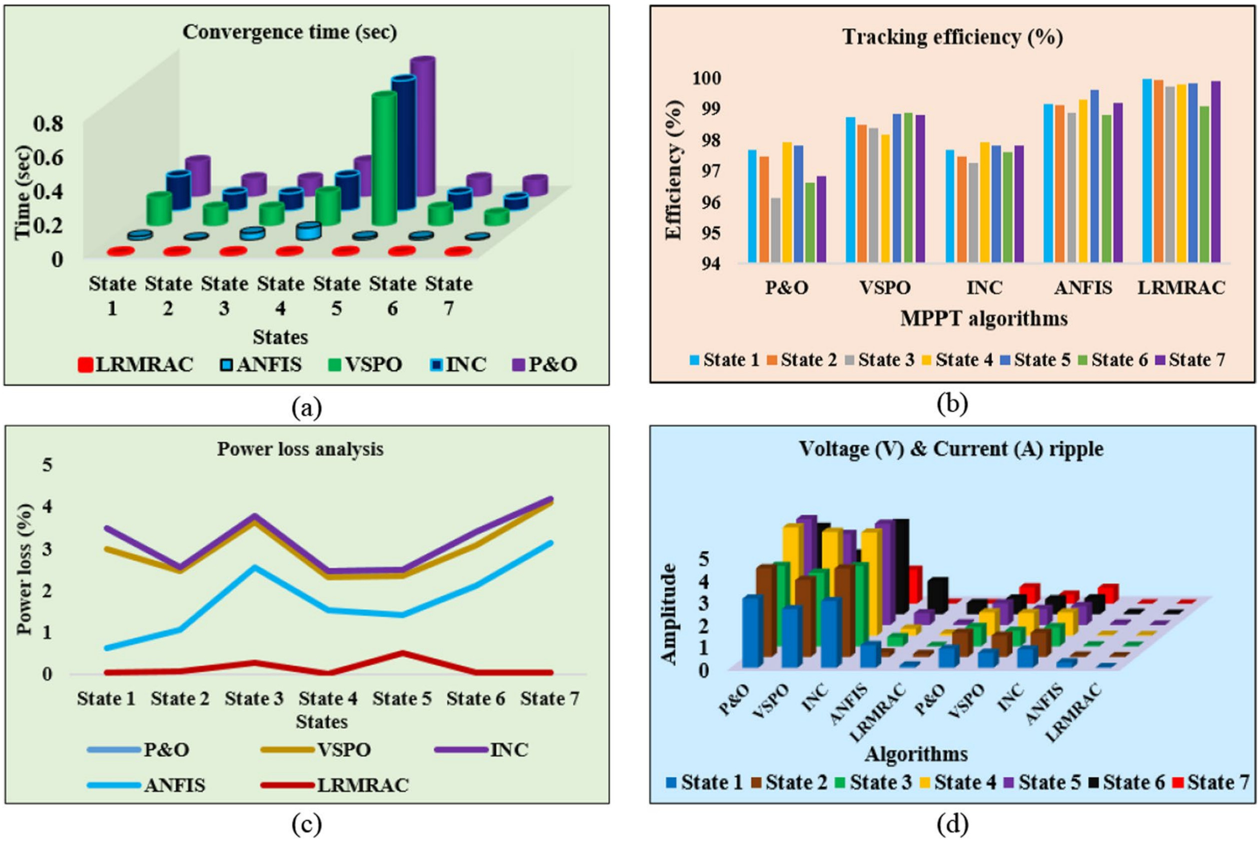

Fig. 15 Comparative evaluation **a** convergence time **b** tracking efficiency **c** power loss **d** voltage and current ripples

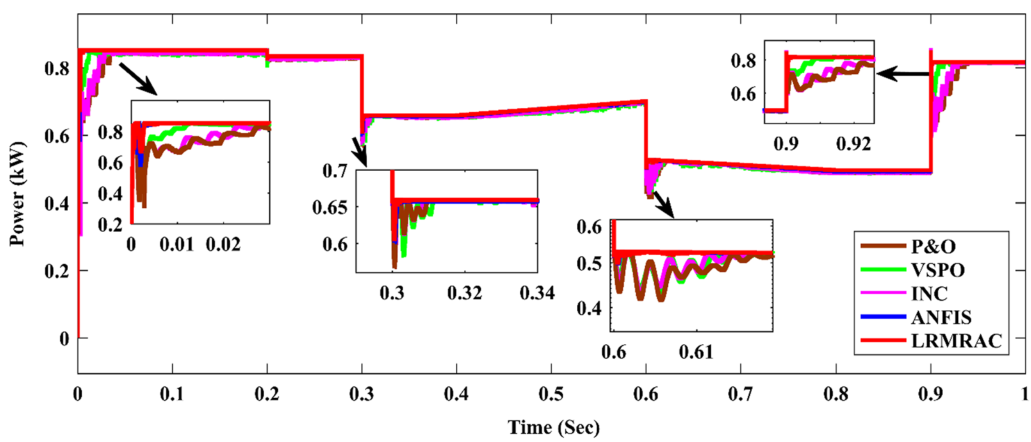

Fig. 16 PV power using the five MPPT algorithms while temperature and radiation change at once

in states 1–7, respectively. While considering the proposed LRMRAC technique, the speed in following the MPP are very fast and the times are 0.0037 s, 0.0033 s, 0.004 s, 0.0054 s, 0.003 s, 0.003 s and 0.0037 s in states 1 to 7, respectively. The tracking efficiencies are between 95.81 and 98.48% for P&O, 95.83–98.46% for INC, 95.81–98.66% for VSPO, 96.05–99.66% for ANFIS, and 97.10–99.96% for the proposed technique. Comparative analysis of the proposed controller with other state-of-the-art MPPT techniques is displayed through a web diagram as shown in Fig. 18. Visual representation clearly illustrates the superiority of the proposed MPPT

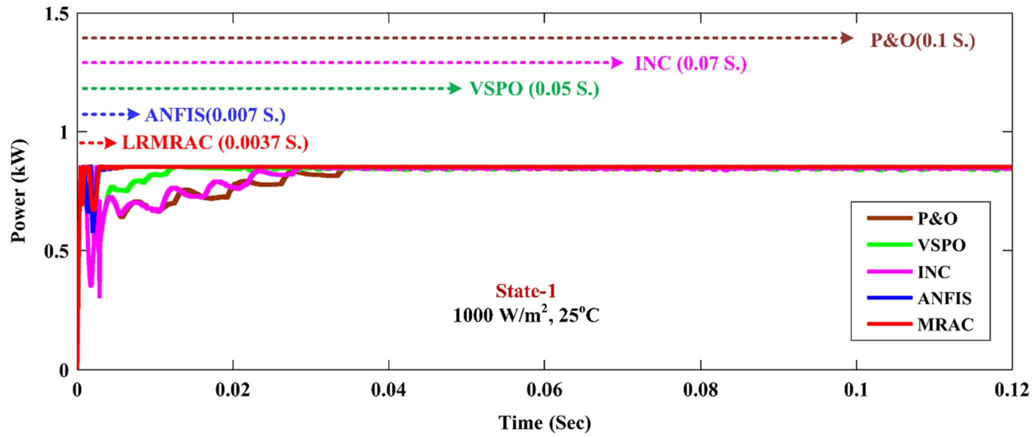

Fig. 17 Speed of the different MPPT algorithms while temperature, and radiation change at once

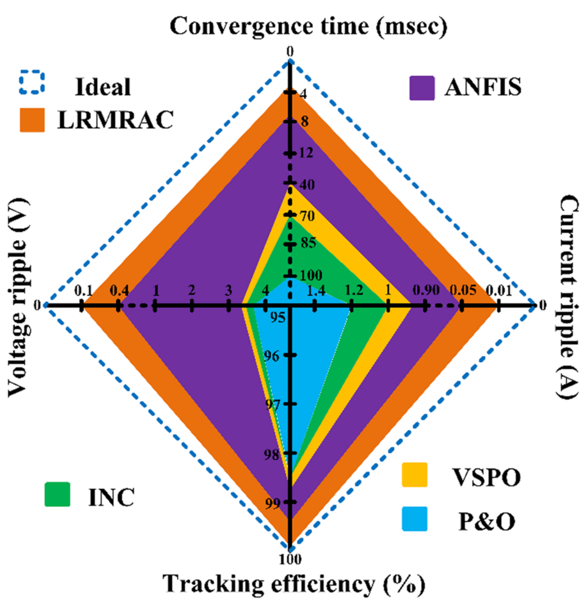

Fig. 18 Visualization demonstrating the merits of the suggested method **a** convergence time **b** current ripple **c** tracking efficiency **d** voltage ripple

algorithm in terms of convergence time, tracking time, and voltage and current ripple.

Time domain analysis is carried out to confirm the effectiveness of the proposed controller using parameters such as settling time, overshoot, rise time and peak time. The rise time of the system is the time necessary to respond to rising from 10 to 90% of final value for an overdamped system, and from 0 to 100% for an underdamped system. The peak time is the length of time needed for the response to reach its first peak, also known as its first peak overshoot. Peak overshoot is defined as the difference between the first-time peak and steady output. The settling time is the length of time needed to attain and maintain its position within the permissible range (2–5%) of its ultimate value. Table 3 compares and summarises the performances of each algorithm in different time domain parameters. From the comparative analysis in all seven states, it is concluded that settling time, rise time, peak time and overshoot of the proposed controller are less than other state-of-the-art techniques. Hence, it is further proved that the proposed controller has a lower convergence time.

6.1.3 Slow variations in radiation, temperature, and load profile

In this scenario, the solar radiation, temperature and load profiles are simultaneously changed, and slow variations are considered. The radiation profile starts from 800 W/m^2 for 1 s and then decreases slowly to 400 W/m^2 over the next second. Likewise, the temperature profile initiates at 25 °C within 1 s and then increases to 30 °C for the remaining second. At the same time, the load value starts from 20 Ω for 1 s for state 1 and increases to 25 Ω for 1 s in state 2. Figure 19 depicts the behaviour of the five MPPT approaches during the slow variations in atmospheric conditions in terms of PV power.

Based on Fig. 19 and its corresponding zoom view, the ripple around the MPP is the highest for the INC, VSPO, and P&O methods, and is reduced for the ANFIS method though at the expense of not being able to achieve MPP. The ripple contents of P&O, INC, VSPO, and ANFIS are 14.8 W, 15.2 W, 20.3 W, and 2.6 W, respectively, whereas the proposed LRMRAC is ripple-free near the MPP across the two states. It can be concluded that P&O, VSPO, and INC take the longest time to follow the MPP, at nearly 0.35 s. For comparison, ANFIS takes 0.02 s while the proposed method takes only 3.2 ms during slow variations. The average power for P&O, VSPO, INC,

Table 3 Time domain analysis of the five approaches in seven states using various parameters

MPPT Techniques	State 1	State 2	State 3	State 4	State 5	State 6	State 7
Settling time (ms)							
P&O	100	43	30	37	16	10	42
VSPO	50	30	23	26	14	20	15
INC	70	34	25	29	15	11	34
ANFIS	07	04	08	8.9	05	4.2	5.8
LRMRAC	3.7	3.3	04	5.4	03	3	3.7
Overshoot (kW)							
P&O	0.542	0.465	0.465	0.428	0.396	0.402	0.430
VSPO	0.541	0.464	0.463	0.404	0.391	0.399	0.420
INC	0.542	0.465	0.465	0.427	0.396	0.402	0.430
ANFIS	0.121	0.137	0.020	0.176	0.124	0.111	0.102
LRMRAC	0.108	0.114	0.012	0.017	0.094	0.081	0.090
Peak time (ms)							
P&O	1.782	1.727	1.767	1.820	4.253	4.358	1.772
VSPO	1.779	1.726	1.727	1.818	4.100	4.242	1.676
INC	1.792	1.728	1.767	1.820	4.107	4.262	1.772
ANFIS	0.627	0.585	1.385	1.437	2.388	2.443	1.964
LRMRAC	0.504	0.509	0.874	1.003	1.281	1.903	1.364
Rise time (ms)							
P&O	0.900	0.915	0.810	0.670	2.770	2.770	1.006
VSPO	0.895	0.913	0.808	0.668	2.760	2.730	0.814
INC	0.898	0.918	0.811	0.670	2.770	2.770	0.910
ANFIS	0.435	0.312	0.621	0.762	1.815	1.668	0.751
LRMRAC	0.295	0.272	0.310	0.402	0.268	0.268	0.295

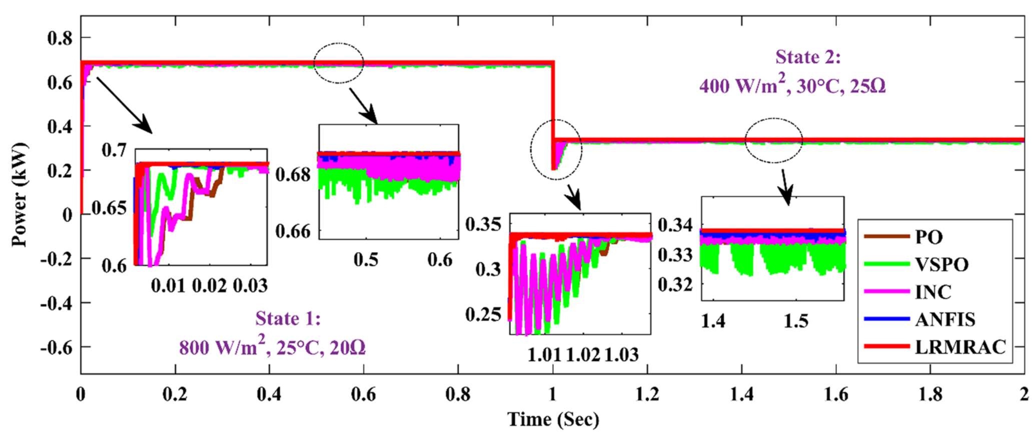

Fig. 19 PV power behaviours of the five MPPT controllers under slow variations of radiation, temperature and load profile

and ANFIS are 648.7 W, 649.1 W, 648.7 W, and 670.7 W, respectively, while the proposed controller generated 680.7 W in state 1.

Hence, the outcomes demonstrate the superiority, robustness, and speed of response of the proposed controller, even with slow variations in temperature, radiation, and load.

6.2 Level-II uncertainty

6.2.1 Partial shading conditions

The suggested MPPT scheme is used for a standalone PV system to track the maximum possible power under PSC in MATLAB/Simulink. Under four distinct shading patterns, the proposed controller's performance is compared to those of P&O and ANFIS controllers. The performance of the proposed method is assessed and compared to that existing methods, using performance indicators including GMPP tracking and shading losses.

In spite of advances in PV technology, partial shading has a negative impact on the system and results in power loss. Shading loss is the term used to describe the power loss caused by shading, which is defined as the difference in power between total maximum power obtained under PSC ($p_{mpp,shading}$) and under STC ($p_{mpp,without\ shading}$) [30], as:

$$p_{mpp,\,shading\ loss} = p_{mpp,without\ shading} - p_{mpp,shading} \tag{42}$$

The three PV modules in the proposed system are linked in series in the present study, resulting in a maximum power output of 1.05 kW. To create varied shade patterns, the modules are excited at different amounts of radiation. Figure 20a–d show the different shading possibilities with their irradiation levels as patterns 1, 2, 3 and 4, respectively.

The P–V characteristics under various shading patterns are displayed in Fig. 21a, while Fig. 21b illustrates the PV power for P&O, ANFIS, and LRMRAC approaches under various shading patterns. Table 4 shows the LMPP and GMPP rates under different shading arrangements. The detailed steady-state responses of different MPPT approaches are given in Table 5, and the associated shading losses are shown in Table 6. The considered cases are discussed in detail in the following paragraphs.

Pattern 1 In this pattern, the LRMRAC algorithm tracks the highest maximum power of 998 W, with no oscillation around GMPP, and the least amount of power is lost through shading, i.e., 51 W. ANFIS tracks 930.5W, while classical P&O MPPT records only 842.3 W, which is the lowest power tracking and its shading losses are the highest at 206.7 W.

Pattern 2 The proposed LRMRAC-based MPPT method captures the highest maximum power of 448.1 W and the lowest shading losses of 600.9 W when compared to other MPPT techniques. In addition, the LRMRAC-MPPT approach tracks power more efficiently than other algorithms in this pattern.

Pattern 3 The proposed approach harvests 115.77 W maximum power, and there is no oscillation around GMPP. The least amount of power is lost because of shading, i.e., 933.23 W. It is noted that ANFIS tracks 59.73 W of power, whereas the classical P&O MPPT algorithm tracks 45.21 W, making it the least effective with the largest shading power losses of 1003.79 W.

Pattern 4 The LRMRAC algorithm generates a highest possible power of 540.3 W, and detects no oscillation around GMPP. The shading losses of 508.7 W are also the lowest. In contrast, ANFIS tracks 490.9 W of power,

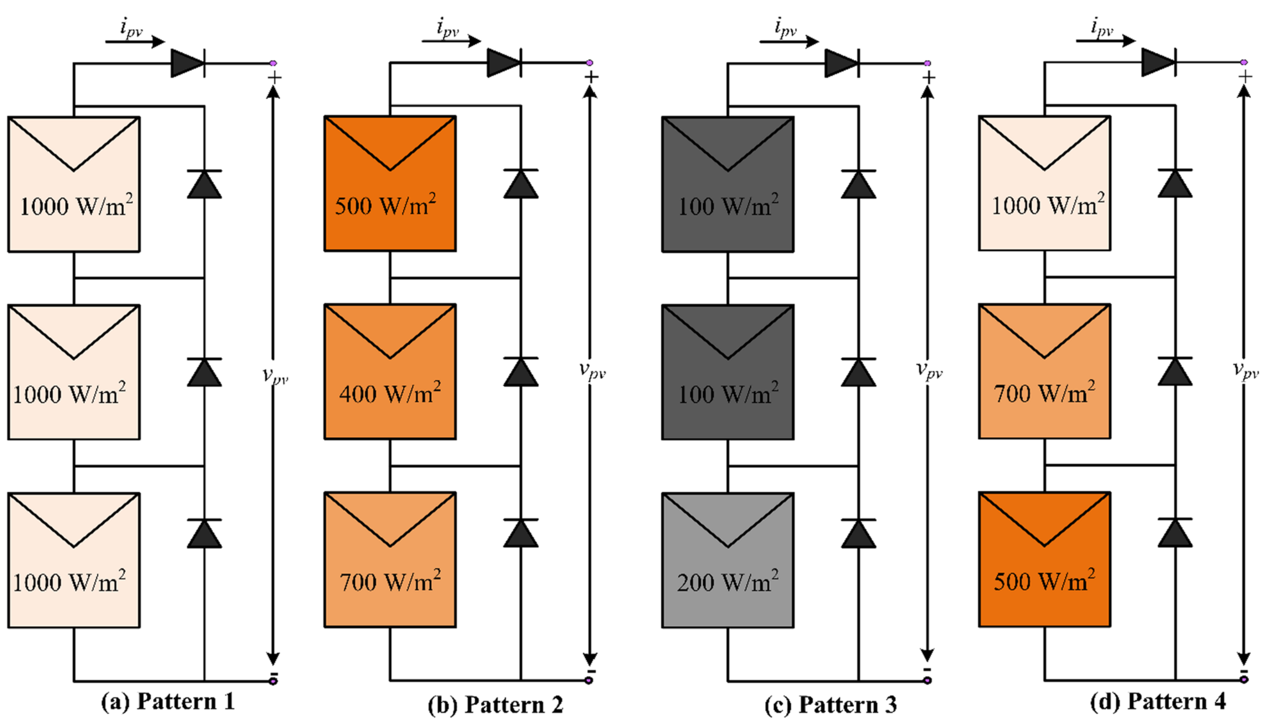

Fig. 20 PV module shading patterns for the proposed scheme

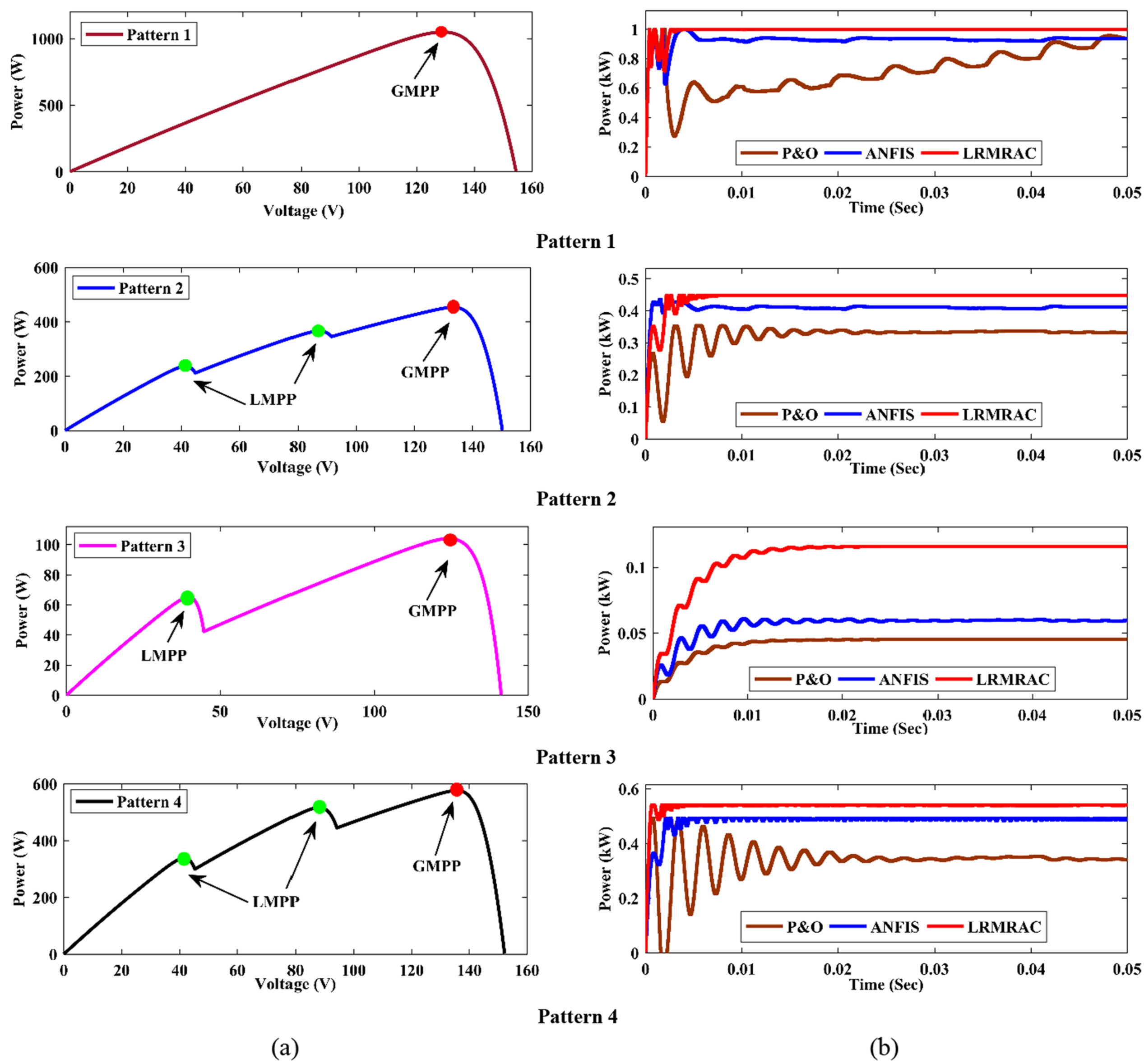

Fig. 21 **a** P–V curve **b** The PV power for P&O, ANFIS, and LRMRAC scheme in various shading patterns

Table 4 Power at GMPP and LMPP under the four different shading patterns

	Pattern 1	Pattern 2	Pattern 3	Pattern 4
GMPP (W)	1049	453.3	124.1	576.4
LMPP (W)	–	366.1, 236	65	516.5, 338.2

whereas the classical P&O MPPT algorithm tracks 340.8 W with the largest shading losses of 708.2 W.

Tables 5 and 6 clearly show that the proposed technique harvests the maximum power and has the least amount of shading losses under all considered conditions. The traditional P&O approach harvests the least amount of maximum power with the highest shading losses in all four patterns. Comparative analysis of tracked power and shading losses for the three approaches under the four patterns are illustrated in Figs. 22 and 23, respectively.

6.3 Level-III uncertainty

6.3.1 Validation of proposed scheme using OP4510 real-time simulator

The performance of the LRMRAC is tested in the lab using an OPAL-RT real-time simulator (OP-4510), as shown in Fig. 24. The proposed method is first simulated on the host-PC running the RT-LAB software

Table 5 Steady-state response of different MPPT approaches under study

Shading Pattern	Technique	Power at MPP (W)	Voltage at MPP (V)	Current at MPP (A)
Pattern 1 (1000,1000,1000 W/m^2)	P&O	842.3	112.00	7.52
	ANFIS	930.5	114.03	8.16
	LRMRAC (Proposed)	998.0	119.37	8.36
Pattern 2 (500, 400, 700 W/m^2)	P&O	334.4	68.10	4.91
	ANFIS	409.9	80.37	5.10
	LRMRAC (Proposed)	448.1	83.60	5.36
Pattern 3 (100, 100, 200 W/m^2)	P&O	45.21	26.24	1.72
	ANFIS	59.73	33.31	1.79
	LRMRAC (Proposed)	115.77	67.31	1.72
Pattern 4 (1000, 700, 500 W/m^2)	P&O	340.8	39.17	8.70
	ANFIS	490.9	58.86	8.34
	LRMRAC (Proposed)	540.3	63.41	8.52

Table 6 Shading loss (W) in various MPPT approaches under study

	Pattern-1	Pattern-2	Pattern-3	Pattern-4
P&O	206.7 W	714.6 W	1003.79 W	708.2 W
ANFIS	118.5 W	639.1 W	989.27 W	558.1 W
LRMRAC (Proposed)	51 W	600.9 W	933.23 W	508.7 W

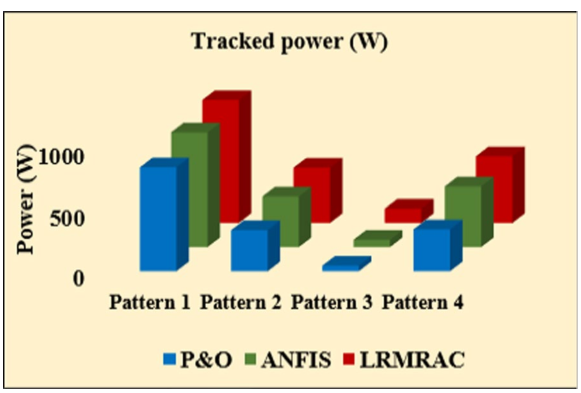

Fig. 22 Comparative analysis of tracked power

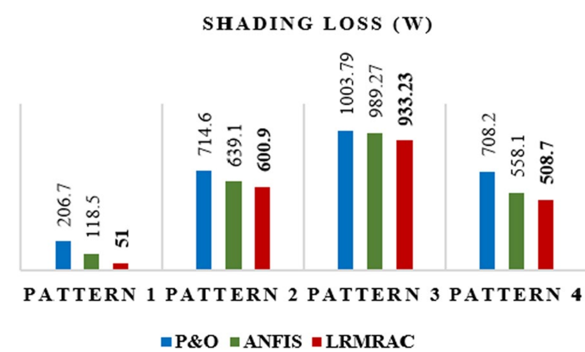

Fig. 23 Comparative analysis of shading loss

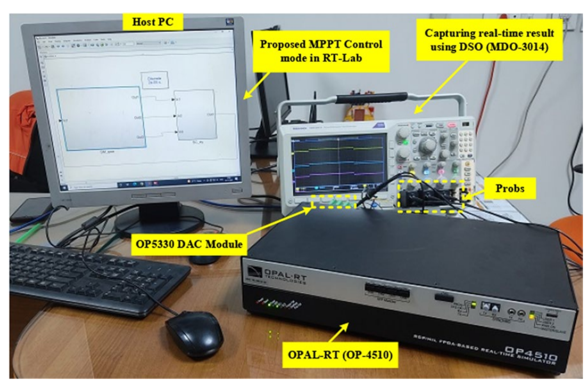

Fig. 24 Laboratory based experimental setup

of the OPAL-RT simulator. Then an oscilloscope and OP5330 DAC are used to record the real-time results from the OP4510 simulator. On DSO, the signals including v_{pv}, i_{pv}, and p are observed and recorded in three different weather situations. Figure 25 shows the experimental results under varied radiation, Fig. 26 depicts the experimental outcomes under changing temperature and fixed radiation (1000 W/m^2), while Fig. 27 depicts the results with simultaneously varying radiation and temperature levels. As seen, low-oscillation tracking of the MPP is achieved using the proposed control approach. In addition, the MPP is accurately monitored despite a sudden increase in radiation from 500 to 1000 W/m^2 and an increase in temperature from 25 to 35 °C.

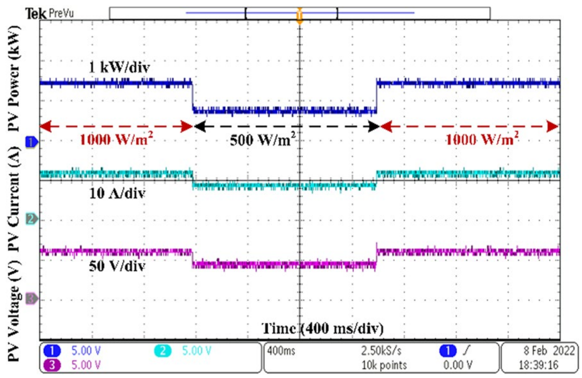

Fig. 25 PV voltage, power and current response for the proposed method in the presence of changing radiation

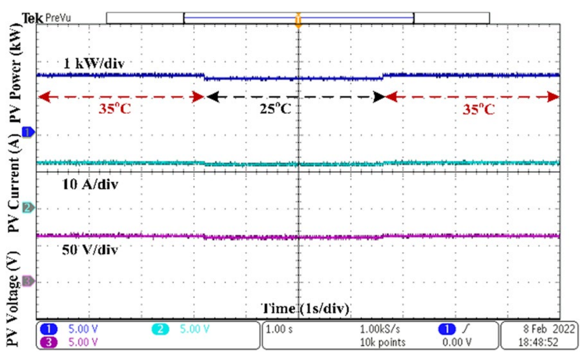

Fig. 26 PV voltage, power and current response for the proposed method in the presence of changing temperature

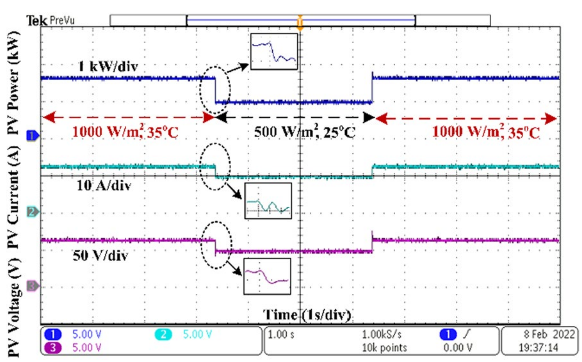

Fig. 27 PV voltage, power and current response for the proposed method in the presence of changing both

Initializing a radar chart makes comparisons easier, while evaluating controller performance is conducted on five key criteria, i.e., efficiency, complexity, steady-state oscillation, tracking time, and PSC operating capability. Figure 28 shows the radar chart diagrams of ten different MPPT approaches. The radar diagram contour is normalised on a scale of 1 (minimum) to 4 (maximum). A method's strength can be seen in the maximum sale, while its weakness can be seen on the minimum scale. Slow and very fast tracking times signify minimum and maximum scales, respectively. When it comes to steady-state oscillation, higher and lower oscillations represent the minimum and maximum scales. For algorithm complexity, easy represents the maximum scale, whereas very difficult represents the minimum scale. The lower and higher efficiencies represent the minimum and maximum scales, while if the algorithm is robust under PSC, it gets the maximum scale. Otherwise, it gets the minimum scale.

A case study is offered here in order to better comprehend the performance assessment process. There are four different categories for tracking speed: slow, medium, fast, and very fast for (> 1 s), (0.1–1 s), (0.1–0.01 s), and (0.01–0.001 s), respectively. Efficiency is classified as very high, high, medium, and low for the ranges of (> 99.50%), (99–99.5%), (98–99%), and (< 98%), respectively. On the spider graph, the large contour area outperforms the small contour area. The complexity, efficiency, speed, accuracy, and environmental impact of the proposed LRMRAC-MPPT scheme have all been proven to be better than the existing methods.

7 Conclusion

A new adaptive method known as Lyapunov-based robust model reference adaptive control (LRMRAC) is presented for MPPT under partially shaded, and slowly and rapidly fluctuating atmospheric conditions. The LRMRAC controller is developed to accomplish the following goals: (i) have simple design and be easy to implement; (ii) reduced oscillation near MPP; (iii) adaptability towards fluctuating atmospheric circumstances; and (iv) exhibit fast tracking response. Probabilistic assessments are carried out using simulation and experimental validation of the proposed controller through various levels of uncertainty. In addition, the LRMRAC controller performance is compared to the cutting edge schemes, i.e., P&O, ANFIS, INC, and VSPO controllers. The LRMRAC-MPPT tracking efficiency ranges from 99.07 to 99.96% for all the considered states, compared to 96.60–97.81% for P&O, 98.16–98.79% for VSPO, 97.23–97.91% for INC, and 98.79–99.27% for ANFIS. The proposed MPPT technique has the lowest tracking power losses of all approaches and negligible oscillation around MPP. In addition, the proposed MPPT technique takes 3.8 ms to reach the MPP, which is about 52 times faster than the classical P&O and INC techniques, 42 times faster than VSPO, and 6 times faster than ANFIS. The LRMRAC-MPPT scheme also has the fewest errors at the MPP. In PSC, the proposed controller performance is compared

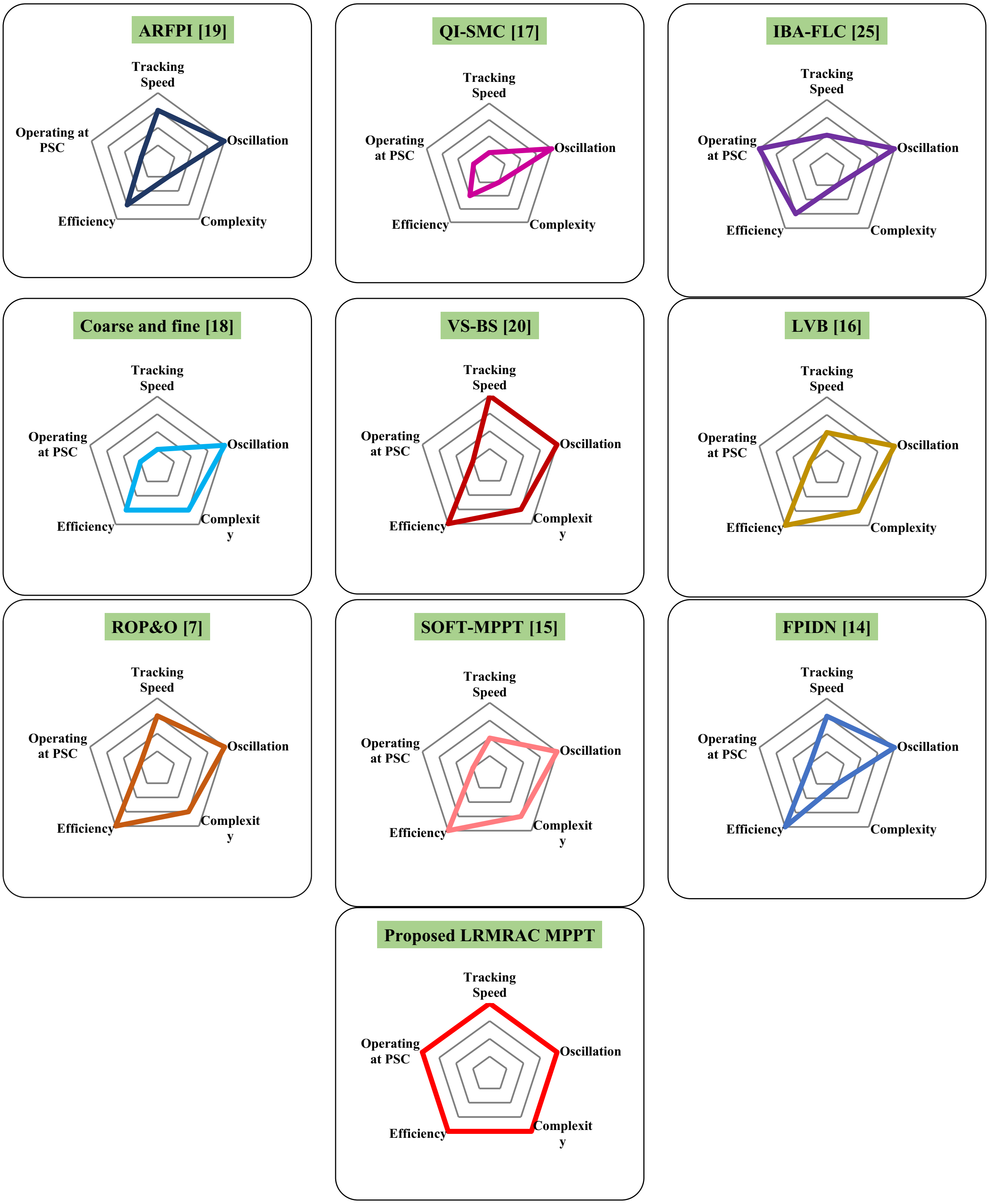

Fig. 28 Radar graphs demonstrating the performance comparison of the different cutting edge MPPT schemes

with P&O and ANFIS with four different shading patterns. GMPP is accomplished in under 10 ms which is the quickest among all MPPT techniques. In each pattern, the proposed controller has the minimum shading losses whereas P&O and ANFIS have significantly higher power losses. Also, it harvests the maximum power rapidly and is ripple-free. Finally, the practicality of the proposed method is demonstrated by real-time validation utilising the OPAL-RT simulator (OP-4510). Thus, the above results validate the consistency of the proposed LRMRAC-MPPT scheme under different environmental uncertainty.

Abbreviations

GMPPT	Global maximum power point tracking
ANFIS	Adaptive neuro fuzzy inference system
VSPO	Variable step perturbation and observation
PSC	Partial shading condition
FPIDN	Fuzzy aided integer order proportional integral derivative with filter
SOFT	Steady output and fast tracking
LVB	Load voltage based MPPT
ROP&O	Reduced oscillation P&O
ARFPI	Adaptive robust fuzzy proportional-integral
VS-BS	Variable step backstepping
PS-FW	Particle swarm-fireworks
IBA	Improved bat algorithm
P–V	Power–voltage
PV	Photovoltaic

Acknowledgements
Not applicable

Author contributions
SM proposed the idea, formulated the approach, carried out the simulation studies and finished the manuscript writing. DKS carried out simulation studies and improved the paper quality. AKA provided guidance and reviewed the manuscript. All authors read and approved the final manuscript.

Funding
Not applicable.

Availability of data and materials
Not applicable.

Declarations

Competing interests
The authors declare that they have no known competing financial interests or personal relationships that could have appeared to influence the work reported in this paper.

Received: 2 September 2022 Accepted: 27 March 2023
Published online: 05 April 2023

References

1. Gielen, D., Boshell, F., Saygin, D., Bazilian, M. D., Wagner, N., & Gorini, R. (2019). The role of renewable energy in the global energy transformation. *Energy Strategy Reviews, 24*, 38–50.
2. Singh, D. K., Akella, A. K., & Manna, S. (2022). Deterministic and probabilistic analysis of different empirical models to estimate monthly mean diffuse solar radiation for composite climatic region of India. *Environmental Progress and Sustainable Energy, 41*(6), e13917. https://doi.org/10.1002/ep.13917
3. Manna, S., Akella, A. K., & Singh, D. K. (2023). Implementation of a novel robust model reference adaptive controller-based MPPT for stand-alone and grid-connected photovoltaic system. *Energy Sources, Part A: Recovery, Utilization, and Environmental Effects, 45*(1), 1321–1345. https://doi.org/10.1080/15567036.2023.2178550
4. Mao, M., Cui, L., Zhang, Q., Guo, K., Zhou, L., & Huang, H. (2020). Classification and summarization of solar photovoltaic MPPT techniques: A review based on traditional and intelligent control strategies. *Energy Reports, 6*, 1312–1327. https://doi.org/10.1016/j.egyr.2020.05.013
5. Wasim, M. S., Amjad, M., Habib, S., Abbasi, M. A., Bhatti, A. R., & Muyeen, S. M. (2022). A critical review and performance comparisons of swarm-based optimization algorithms in maximum power point tracking of photovoltaic systems under partial shading conditions. *Energy Reports, 8*, 4871–4898. https://doi.org/10.1016/j.egyr.2022.03.175
6. Ali, M. N., Mahmoud, K., Lehtonen, M., & Darwish, M. M. F. (2021). An efficient fuzzy-logic based variable-step incremental conductance mppt method for grid-connected PV systems. *IEEE Access, 9*, 26420–26430. https://doi.org/10.1109/ACCESS.2021.3058052
7. Pathak, P. K., Yadav, A. K., & Alvi, P. A. (2022). Reduced oscillations based perturb and observe solar maximum power point tracking scheme to enhance efficacy and speed of a photovoltaic system. *Journal of Engineering Research*. https://doi.org/10.36909/jer.13569
8. Bisht, R., & Sikander, A. (2022). An improved method based on fuzzy logic with beta parameter for PV MPPT system. *Optik (Stuttg), 259*, 168939. https://doi.org/10.1016/j.ijleo.2022.168939
9. Laxman, B., Annamraju, A., & Srikanth, N. V. (2021). A grey wolf optimized fuzzy logic based MPPT for shaded solar photovoltaic systems in microgrids. *International Journal of Hydrogen Energy, 46*(18), 10653–10665.
10. Tavakoli, A., & Forouzanfar, M. (2020). A self-constructing Lyapunov neural network controller to track global maximum power point in PV systems. *International Transactions on Electrical Energy Systems, 30*, 12391. https://doi.org/10.1002/2050-7038.12391
11. Elnozahy, A., Yousef, A. M., Abo-Elyousr, F. K., Mohamed, M., & Abdelwahab, S. A. M. (2021). Performance improvement of hybrid renewable energy sources connected to the grid using artificial neural network and sliding mode control. *Journal of Power Electronics, 21*, 1166–1179.
12. Mirza, A. F., Mansoor, M., Ling, Q., Khan, M. I., & Aldossary, O. M. (2020). Advanced variable step size incremental conductance MPPT for a standalone PV system utilizing a GA-tuned PID controller. *Energies (Basel), 13*(16), 4153. https://doi.org/10.3390/en13164153
13. Harrag, A., & Messalti, S. (2019). PSO-based SMC variable step size P&O MPPT controller for PV systems under fast changing atmospheric conditions. *International Journal of Numerical Modelling: Electronic Networks, Devices and Fields, 32*(5), e2603. https://doi.org/10.1002/jnm.2603
14. Srinivasarao, P., Peddakapu, K., Mohamed, M. R., Deepika, K. K., & Sudhakar, K. (2021). Simulation and experimental design of adaptive-based maximum power point tracking methods for photovoltaic systems. *Computers and Electrical Engineering, 89*, 106910. https://doi.org/10.1016/j.compeleceng.2020.106910
15. Bhattacharyya, S., Kumar, P. D. S., Samanta, S., & Mishra, S. (2021). Steady output and fast tracking MPPT (SOFT-MPPT) for P&O and InC algorithms. *IEEE Transactions on Sustainable Energy, 12*(1), 293–302. https://doi.org/10.1109/TSTE.2020.2991768
16. Kumar, V., Ghosh, S., Naidu, N. K. S., Kamal, S., Saket, R. K., & Nagar, S. K. (2021). Load voltage-based MPPT technique for standalone PV systems using adaptive step. *International Journal of Electrical Power and Energy Systems, 128*, 106732. https://doi.org/10.1016/j.ijepes.2020.106732
17. Aminnejhad, H., Kazeminia, S., & Aliasghary, M. (2021). Robust sliding-mode control for maximum power point tracking of photovoltaic power systems with quantized input signal. *Optik (Stuttg), 247*, 167983. https://doi.org/10.1016/j.ijleo.2021.167983
18. Kavya, M., & Jayalalitha, S. (2022). A novel coarse and fine control algorithm to improve maximum power point tracking (MPPT) efficiency in photovoltaic system. *ISA Transactions, 121*, 180–190. https://doi.org/10.1016/j.isatra.2021.03.036
19. Kumar, V., Mitra, A., Shaklya, O., Sharma, S., & Rana, K. P. S. (2022). An adaptive robust fuzzy PI controller for maximum power point tracking of photovoltaic system. *Optik (Stuttg), 259*, 168942. https://doi.org/10.1016/j.ijleo.2022.168942

20. Charaabi, A., Zaidi, A., Barambones, O., & Zanzouri, N. (2022). Implementation of adjustable variable step based backstepping control for the PV power plant. *International Journal of Electrical Power and Energy Systems, 136*, 107682. https://doi.org/10.1016/j.ijepes.2021.107682
21. Shang, L., Zhu, W., Li, P., & Guo, H. (2018). Maximum power point tracking of PV system under partial shading conditions through flower pollination algorithm. *Protection and Control of Modern Power Systems, 3*, 38. https://doi.org/10.1186/s41601-018-0111-3
22. Iqbal, B., Nasir, A., & Murtaza, A. F. (2021). Stochastic maximum power point tracking of photovoltaic energy system under partial shading conditions. *Protection and Control of Modern Power Systems, 6*, 30. https://doi.org/10.1186/s41601-021-00208-9
23. Chai, L. G. K., Gopal, L., Juwono, F. H., Chiong, C. W. R., Ling, H. C., & Basuki, T. A. (2021). A novel global MPPT technique using improved PS-FW algorithm for PV system under partial shading conditions. *Energy Conversion and Management, 246*, 114639. https://doi.org/10.1016/j.enconman.2021.114639
24. Ali, Z. M., Alquthami, T., Alkhalaf, S., Norouzi, H., Dadfar, S., & Suzuki, K. (2022). Novel hybrid improved bat algorithm and fuzzy system based MPPT for photovoltaic under variable atmospheric conditions. *Sustainable Energy Technologies and Assessments, 52*(B), 102156. https://doi.org/10.1016/j.seta.2022.102156
25. Manna, S., Singh, D. K., Akella, A. K., Abdelaziz, A. Y., & Prasad, M. (2022). A novel robust model reference adaptive MPPT controller for photovoltaic systems. *Scientia Iranica*. https://doi.org/10.24200/sci.2022.59553.6312
26. Khanna, R., Zhang, Q., Stanchina, W. E., Reed, G. F., & Mao, Z. H. (2014). Maximum power point tracking using model reference adaptive control. *IEEE Transactions on Power Electronics, 29*, 1490–1499.
27. Manna, S., Akella, A. K., & Singh, D. K. (2022). A novel MRAC-MPPT scheme to enhance speed and accuracy in PV systems. *Iranian Journal of Science and Technology, Transactions of Electrical Engineering*. https://doi.org/10.1007/s40998-022-00542-0
28. Saidi, K., Maamoun, M., & Bounekhla, M. (2019). A new high performance variable step size perturb-and-observe MPPT algorithm for photovoltaic system. *International Journal of Power Electronics and Drive Systems (IJPEDS), 10*(3), 1662–1674. https://doi.org/10.11591/ijpeds.v10.i3.pp1662-1674
29. Alice Hepzibah, A., & Premkumar, K. (2020). ANFIS current–voltage controlled MPPT algorithm for solar powered brushless DC motor based water pump. *Electrical Engineering, 102*, 421–435. https://doi.org/10.1007/s00202-019-00885-8
30. Verma, P., Garg, R., & Mahajan, P. (2020). Asymmetrical fuzzy logic control-based MPPT algorithm for standalone photovoltaic systems under partially shaded conditions. *Scientia Iranica, 27*, 3162–3174. https://doi.org/10.24200/SCI.2019.51737.23